

Simulation and theory of two-phase flow in porous media

Martin Blunt* and Michael J. King

BP Research Centre, Chertsey Road, Sunbury-on-Thames, Middlesex, TW16 7LN United Kingdom

Harvey Scher

BP Research Center, 4440 Warrensville Center Road, Cleveland, Ohio 44128-2837

(Received 14 August 1991; revised manuscript received 21 August 1992)

A three-dimensional network model of a porous medium is used to compute relative permeabilities and capillary pressures in drainage and imbibition. In contrast, the invasion-percolation model of drainage with trapping does not make a sensible prediction for the relative permeability of either the displaced or injected phases since it fails to represent the fluid connectivity correctly. We describe two realistic trapping mechanisms which overcome this difficulty by representing the flow of the wetting phase along irregularities in the pore-grain surface. In imbibition, we simulate the rate-dependent competition between bulk filling of pores and film flow and show how different displacement mechanisms affect relative permeability. We verify percolation-theory results for the effects of buoyancy forces on trapped saturation by simulation and derive an expression for the correlation length in displacements perturbed by viscous forces. We can then demonstrate how relative permeabilities measured in quasistatic systems at capillary equilibrium are still meaningful in larger-scale displacements where viscous forces predominate.

PACS number(s): 47.55.Mh, 64.60.Ak, 47.55.Kf

I. INTRODUCTION

There has been much study of two-phase flow using numerical networks to represent the pore structure [1–21]. These simulations have been complemented by experiments in idealized two-dimensional porous media [4,8,17,18,22–26] where different pore-scale displacement mechanisms could be seen. There have also been several theoretical and numerical studies relating capillary-dominated flow to percolation theory [27–34].

Whilst the displacement mechanisms in model two-dimensional (2D) experimental porous media are well established [22,35,36], there is still considerable confusion in the literature as to the appropriate flow behavior necessary to describe flow through three-dimensional rock. By using a numerical network to represent the pore structure, we can clearly demonstrate that simple site or bond percolation models are inadequate representations of either drainage (invasion by a nonwetting fluid) or imbibition (injection of a wetting fluid).

The invasion-percolation model of drainage with trapping accurately reproduces the configuration of filled pores seen in two-dimensional experiments, but does not make a sensible prediction for the overall hydraulic conductivity (relative permeability) of either the displaced or injected phases in three dimensions as it fails to represent the fluid connectivity correctly. We show how to modify the model to account for the flow of the wetting phase along small crevices in the pore-grain surface and describe two realistic trapping mechanisms.

As shown by the experiments of Lenormand and Zarccone [22], a percolation model of imbibition is typically never appropriate and the displacement is rate dependent, even when viscous forces are neglected, as there is a

competition between an advancing and swelling wetting film, and the bulk filling of tubes and pores. We simulate these processes in a three-dimensional network and show their affects on relative permeability.

Percolation theory is thus restricted to a limited set of circumstances, namely drainage and the trapping of both wetting and nonwetting phases. We apply scaling arguments to valid models of fluid flow and demonstrate their validity by simulation.

Relative permeability and capillary pressure are mesoscopic parameters in empirical differential equations which describe the average transport behavior of multiphase flow. They are well-defined properties for steady-state capillary-dominated displacements, but it is not obvious how the concept can be applied to flow influenced by viscous and buoyancy forces. Wilkinson postulated [33,34] that these forces introduce a finite correlation length into a percolation description of trapping. We verify this picture for buoyancy by simulation. We then derive the viscous correlation length. The relative permeability is well defined if measured in a region where the saturation distribution is locally homogeneous, that is over a scale greater than the correlation length and smaller than the macroscopic size of the displacement pattern in which the averaged saturation changes appreciably. This means that relative permeability is still a valid concept in displacements which are dominated by viscous forces on the large scale, as long as the fluid configuration is controlled mainly by capillary forces at the pore scale, which is almost always the case in experimental and reservoir flows in porous media.

Fluid displacements in aquifers and oil reservoirs typically occur over lengths of several kilometers. The large-scale behavior is controlled by a flow field governed by viscous and buoyancy forces and the geological

heterogeneity of the system. The macroscopic flow may be predicted from a numerical computation of the flow with estimates for the spatially varying fluid and rock properties. However, at the pore scale it is capillary forces which control the fluid configuration and the hydraulic conductivity of each phase. The use of relative permeabilities in a multiphase Darcy law bridges the gap between pore-scale displacement phenomena and the macroscopic flow by incorporating the relevant microscopic dynamics in a differential equation which may be solved on a larger system. It is for this reason that a clear understanding of relative permeability and how it changes in different circumstances is important.

II. REPRESENTING THE PORE SPACE

The pore space of a rock consists of large void spaces between grains, connected by thinner pathways. The surface between the rock and pore space is rough and continuous. The large voids can contain much fluid, and so a phase which fills these regions will have a high saturation. The thinner connections present the major barriers to flow, which affects the permeability. The rough pore-grain surface controls film transport of the wetting phase. Our numerical network model will attempt to reproduce these features, but is not constructed as a correct and accurate representation of a particular physical system.

We use a *tubes and chambers* model of a porous medium [37]. The void spaces are represented as spherical nodes or pores of a radius r_v , which can vary. The volume of each node is $\frac{4}{3}\pi r_v^3$. The nodes are connected by tubes or throats with a minimum radius r_t , where $r_v > r_t$. The value of r_t for each throat may be different. We define a distribution function $f(r_t)$ such that the fraction of tubes in the network with a radius between r_t and $r_t + dr_t$ is $f(r_t)dr_t$. The throats are modeled as cylindrical tubes of radius r_t and volume $\pi r_t^2 l$, where l is the tube length. The nodes or pores are placed in a simple cubic lattice with tubes joining nearest neighbors.

The surface roughness is not modeled explicitly. However, we do allow a completely wetting phases to permeate the whole system as a thin film as wide as the scale of the roughness (which is usually less than $1 \mu\text{m}$). When we discuss imbibition we will quantify the rate of film flow and its dependence on the degree of roughness.

Figure 1 shows a 2D section through our numerical network. The tubes are simply represented as cylinders whose radii are chosen uniformly from 0 to r_{t0} , where r_{t0} is some referenced radius. The node radii are chosen at random uniformly from r_{t0} to $4r_{t0}$.

III. TWO-PHASE FLOW

A. Capillary equilibrium

Consider two immiscible fluids at rest in a porous medium. If one phase is completely wetting, a thin film will coat all the solid surfaces and thus cover the small ($< 1 \mu\text{m}$) irregularities on the grains. However, there will also be curved surfaces between the two fluids. There is a pressure drop ΔP across the interface because of the surface tension between the fluids:

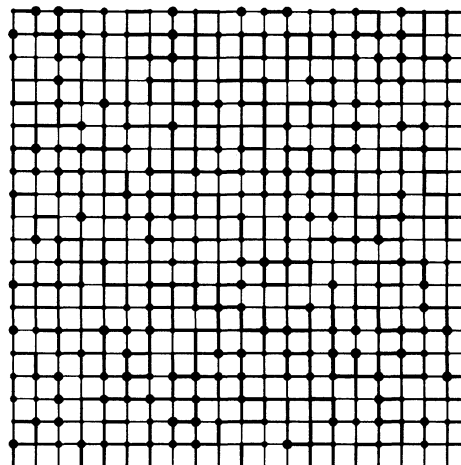


FIG. 1. A two-dimensional cross section through a numerical network model of a porous medium. The pore spaces are arranged on a cubic grid.

$$\Delta P = \gamma \left(\frac{1}{r_1} + \frac{1}{r_2} \right), \quad (3.1)$$

where γ is the surface tension and r_1 and r_2 are the principal radii of curvature of the interface. For a cylindrical throat of radius r

$$\Delta P = - \frac{2\gamma \cos\theta}{r}. \quad (3.2)$$

θ is called the contact angle and is the angle at which the fluid interface approaches the solid surface. If $\theta > 90^\circ$ there is a decrease in pressure across the boundary—the pressure is higher in the nonwetting fluid.

ΔP is very large for any interface in or across tiny crevices in the porous medium, since a radius of curvature will be small. Thus, if there are small channels or corrugations along the pore-grain surface, the wetting phase will preferentially fill them. The wetting phase is thus likely to be hydraulically connected throughout the rock along a network of subpore scale roughness. We show later that consideration of flow through this roughness is vital to be able to make sensible predictions of relative permeability.

B. Relative permeability

We wish to know how the pore-scale fluid dynamics affects macroscopic transport properties in two-phase flow. The most important property is the relative permeability, introduced by Muskat and Meres [38] and Wyckoff and Botset [39]. We start from Darcy's law for single-phase flow [40]:

$$Q = - \frac{K}{\mu} \nabla P, \quad (3.3)$$

where Q is the flow rate per unit cross section of material and ∇P is the pressure gradient. Q and P are macroscopic averages, measured over several pore lengths or more. If this average is taken over a length larger than any correlation length in the pore structure of the medium

(i.e., we measure Q in a statistically homogeneous sample), then the permeability K is a well-defined, intensive property of the rock, which characterizes its flow resistance.

For two-phase immiscible flow, the two fluids reside in different subsections of the pore space. For steady-state flow at an infinitesimal rate, with no interface displacement, then the fluids flow through these separate subsections with no interaction between the phases. In this case there is a hydraulic conductance associated with each phase, which is some fraction of the single phase value K . This fraction is called the relative permeability k_r . k_r depends purely on the fluid configuration at a given saturation. For a given type of displacement k_r may be written as a function of one of the phase saturations only (normally the wetting phase saturation S):

$$Q_w = - \frac{Kk_{rw}(S)}{\mu_w} \nabla P_w, \quad (3.4)$$

$$Q_{nw} = - \frac{Kk_{rnw}(S)}{\mu_{nw}} \nabla P_{nw}, \quad (3.5)$$

where the subscripts w and nw refer to the wetting and nonwetting phases, respectively. The phase pressures P_w and P_{nw} differ by the capillary pressure [41]:

$$P_{cap}(S) = P_{nw} - P_w. \quad (3.6)$$

If the phases are distributed uniformly, then the relative permeabilities and capillary pressure defined above are intensive transport properties describing the system and the displacement processes through it.

The discussion above makes a number of assumptions. First, in two-phase flow, there are interfaces between solid and liquid and liquid and liquid. The boundary conditions are not the same in these two cases. There is no flow at a solid-liquid interface, whereas there will be tangential flow at a liquid-liquid boundary. For instance, if the solid is coated by a wetting film, the nonwetting fluid may be able to move faster through a throat than if the film were absent. This leads to a lubricating effect, which depends on the viscosity ratio of the fluids and may give relative permeabilities greater than 1 [42,43]. For displacements at a finite flow rate, the configuration of fluid is affected by both viscous and capillary forces, and the relative permeabilities will change from their quasistatic values [19,20,44–46]. The significance of viscous effects not only increases with flow rate, but also with the length scale over which the flow Q is measured. Experimentally, dynamic (non-steady-state) displacements are often performed, and the measured relative permeabilities are those consistent with conservation of mass and the observed, nonuniform, saturation profile. These relative permeabilities are then used in reservoir simulators to represent flow in inhomogeneous grid blocks, which are much larger than the size of the experimental system.

It is generally not the case, however, that steady-state relative permeabilities are very different from the quantities actually measured in experiments. For experiments performed at low flow rates on homogeneous samples, the

relative permeability in the vast majority of systems is insensitive to the applied pressure gradient or the size of the sample [46–53]. The effect on relative permeability is only clearly apparent for displacements with a very low surface tension [45] or flow rates about ten times higher than those in typical core floods, and at least 100 times faster than usual reservoir flows [19,20]. We will show why this is the case by demonstrating that viscous forces may be considered as a perturbative influence on capillary equilibrium, and explain how relative permeability may be treated consistently even if viscous forces dominate over large distances.

IV. SIMULATIONS OF DRAINAGE

A. Invasion percolation

Invasion percolation is a model of capillary controlled flow of a fluid into a porous medium first proposed by Chandler *et al.* [28] and Wilkinson and Willemsen [29]. It is similar to the process which is thought to occur in low-rate drainage experiments. Drainage occurs during the formation of a petroleum reservoir when oil, the nonwetting phase, migrates from the source rock into a trap formation, displacing a wetting phase (brine). The injected nonwetting fluid occupies the pore spaces in sequence, at each stage passing through the available throat or pore with the largest radius (lowest capillary pressure). However, retraction from pores is neglected. In this section we will consider the medium originally completely saturated with wetting fluid (for instance, water). Nonwetting fluid (say, oil) is then injected through one face of the system and the fluids escape through the opposite face. The dynamics of invasion percolation has been studied, but an analysis investigating the macroscopic transport properties and their sensitivity to flow in microscopic roughness and trapping has not been provided before.

1. Trapping rules

When the invading phase enters a pore or throat, the displaced fluid needs to escape. If the wetting fluid is continuous throughout the system, then at very low injection rates the wetting phase can escape from any pore or throat by flow in surface roughness to the outlet of the system. This means that no wetting phase is trapped. This mechanism, which results in a virtually zero irreducible water saturation (only thin layers of wetting phase are left in the system), is also equivalent to the displacement of an infinitely compressible fluid, or injection into a vacuum, as in mercury injection experiments. In many experiments the irreducible saturation of wetting phase is typically 10% [46,52,53], which cannot be accounted for solely by surface roughness: some of the wetting phase is trapped in the bulk of the throats and pores. This is certain to happen if the displaced phase is not completely wetting and there is no flow along small irregularities.

We present two simple models of trapping, which we will call *trapping in pores* and *trapping in pores and throats*. If a pore or throat is completely surrounded by

pores filled with nonwetting fluid, then wetting fluid can only be displaced from these regions by flow along corrugations in the pore-grain interface. If we neglect flow in roughness entirely, then the invading fluid can only fill a throat or pore if it lies on a continuous pathway of the system, along which the displaced phase can escape. This is trapping in pores and throats, and is illustrated schematically in Fig. 2. The nonwetting fluid is unable to form loops, since there is always a final link of trapped defending phase in the way. Topologically, the invading fluid has a tree (or, more appropriately, a forest) structure. The fluid pathways can branch, but they cannot merge. The original descriptions of invasion percolation was a modified form of bond percolation which did not carefully describe the process in terms of pores and throats, but this description appears to be consistent with the trapping mechanisms proposed by Chandler *et al.* [28] and Wilkinson and Willemsen [29]. As we will demonstrate later, as well as resulting in a somewhat high irreducible wetting phase saturation, this model predicts vanishing relative permeabilities (even in three dimen-

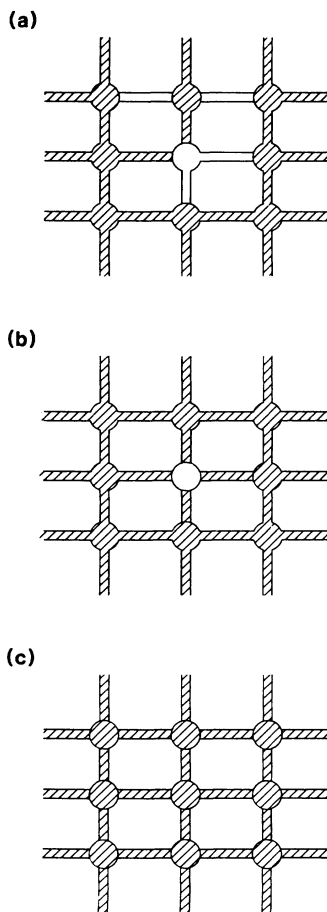


FIG. 2. Trapping mechanisms in drainage. (a) If there is trapping in pores and tubes, no further displacement is possible on the grid illustrated. Loops of the nonwetting fluid cannot be formed. (b) If there is trapping in pores, but not in tubes, tubes connected to a pore filled with wetting fluid may be filled. (c) With no trapping all parts of the network may be filled.

sions). Clearly, in real situations a less severe trapping mechanism must be appropriate to overcome this Zeno paradox.

A new, simple and realistic model of trapping in drainage is to assume that the wetting phase cannot drain from (large) pores surrounded by the invading fluid, but can escape by flow in roughness from (narrower) throats. This mechanism, trapping in pores, is the same as the more restrictive trapping described above, except that throats connected to a pore full of nonwetting fluid may be accessed. The fluid distribution in the pores is just the same as with strict trapping, but drainage out of tubes along small surface irregularities allows loops of invading fluid to form, as illustrated in Fig. 2. This means that more realistic values of relative permeability are obtained.

B. Simulation

The numerical network is a cubic array of cylindrical tubes and spherical pores, as described in Sec. II. Originally the network is full of wetting fluid. Nonwetting fluid is injected into one face of the system. The tubes and pores are filled one at a time. A tube is considered *available* if it contains no injected fluid, but is connected to a pore which does. At each stage the available tube with the largest radius is filled, together with any empty pore attached to it. However, if the displaced fluid in the pore or tube is trapped, as described above, then it cannot be filled. The injection pressure associated with the filling at an infinitesimal flow rate is simply given by capillary equilibrium, Eq. (3.2).

Fluid is injected into one side of the network and escapes through the opposite end. There are periodic boundary conditions on the other sides. *Breakthrough* is defined when the injected fluid first reaches the outlet. Using percolation theory [54,55], the saturation at breakthrough in a system of size L scales as

$$S \sim L^{D-d}, \quad (4.1)$$

where d is the space dimension and D , the fractal dimension, is approximately 1.89 for $d=2$ and 2.5 for $d=3$ [28,29]. For very large L the saturation at breakthrough becomes infinitesimal.

The *terminal point* is defined as the moment when the displacement stops. Without trapping, the entire network is flooded, whereas with trapping, immobile blobs or ganglia of surrounded wetting fluid are left, as illustrated in Fig. 3. Breakthrough represents the percolation threshold of the nonwetting phase, when the fluid first forms a connected pathway across the system. The terminal point, in a process with trapping, represents the percolation threshold of the defending, wetting phase, as it marks the point when the wetting fluid is just unable to escape along a continuous path to the outlet. In two dimensions it is topologically impossible to have two nonintersecting phases which both span the system. This means that in very large networks the terminal point occurs at an infinitesimal saturation beyond breakthrough. Hence, there is no genuine two-phase flow regime, where both fluids have a nonzero relative permeability. In three dimensions, in contrast, we can have two

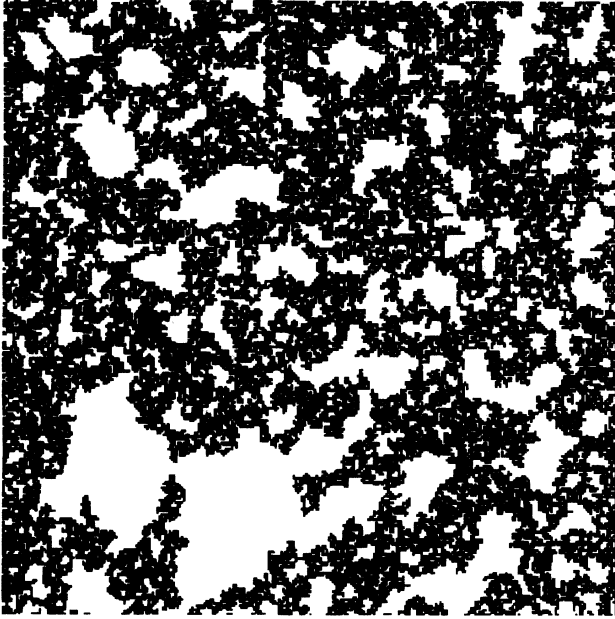


FIG. 3. Invasion percolation with trapping in pores on a 300×300 square network at the terminal point. Only filled pores are shown. Flow is from left to right.

continuous phases. For this reason all the relative permeabilities are computed on three-dimensional networks.

C. Can we use percolation theory?

An analysis using percolation theory relies on being able to use normal percolation exponents in the modified site-bond models with trapping which we have used here

$$S = \frac{z\pi l F_t \int_{r_t}^{\infty} r^2 f(r) dr / 2 \int_{r_t}^{\infty} f(r) dr + \frac{4}{3}\pi F_p \int_0^{\infty} r^3 g(r) dr}{\frac{z}{2}\pi l \int_0^{\infty} r^2 f(r) dr + \frac{4}{3}\pi \int_0^{\infty} r^3 g(r) dr}, \quad (4.4)$$

where z is the coordination number of the lattice and we assume spherical pores and cylindrical tubes of the same length l . If the total volume of the pores is much greater than that of the tubes, then $S \approx F_p$, i.e., the pore occupancy and the saturation are approximately equal.

2. Number of trapped blobs

The quantity which is most likely to be affected by trapping is the distribution of wetting fluid at the terminal point. We investigate the number of isolated clusters (i.e., regions completely surrounded by the invading phase) of wetting fluid containing s pores at the terminal point if we allow trapping. In a pure percolation process, this distribution is the same as the distribution of cluster sizes at the percolation threshold, $N(s) \sim s^{-\tau}$, where $\tau \approx 2.21$ in three dimensions. However, it is possible that trapping enhances the probability of large clusters being

to describe fluid flow. We will make two new direct tests of percolation theory using a drainage model with a correct trapping mechanism.

1. Percolation probability and saturation

Define a percolating probability p as follows: if the thinnest tube filled with nonwetting fluid has a radius r_t , then p is the fraction of all the tubes in the network with a radius larger than r_t . If $f(r)$ is the tube radius distribution, then

$$p = \int_{r_t}^{\infty} f(r) dr. \quad (4.2)$$

For a percolation process, the fraction of filled tubes, $F_t(p) \sim (p - p_c)^\beta$ [54], where p_c is the value of p at breakthrough and the exponent $\beta \approx 0.45$ in three dimensions. p_c depends on the topology of the network, but is independent of $f(r)$. It has the same value, about 0.25, for any cubic network. We hypothesize that the same power law is observed of the pore occupancy: i.e.,

$$F_p \sim (p - p_c)^\beta. \quad (4.3)$$

This relation is tested in Fig. 4, for invasion percolation without trapping on a $32 \times 32 \times 64$ network. The quality of the data is poor, but is consistent with the predicted power law. This means that we can identify pore occupancy with an effective percolation probability, even when the fluid dynamics is controlled by the tubes.

The tubes are filled in order of radius, while the pores are filled irrespective of size, if the pores are larger than the tubes, and there is no correlation in the pore and tube size distributions. Define $f(r)$ and $g(r)$ as the tube- and pore-radius distribution functions, respectively; then the saturation S is

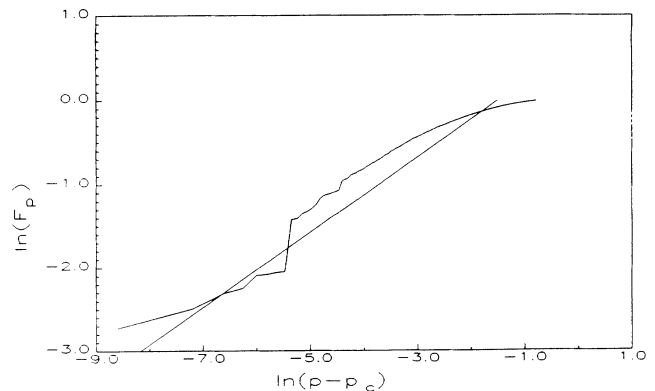


FIG. 4. Pore occupancy against effective percolation probability on a $32 \times 32 \times 64$ network for invasion percolation without trapping. The straight line is the prediction from percolation theory.

left behind, and the exponent could be lower in invasion percolation. We consider the quantity

$$M(s) = \sum_s s N(s) \sim s^{-\tau+2}. \quad (4.5)$$

Figure 5 shows graphs of $M(s)$ from simulations of invasion percolation with trapping in pores, and networks of size $4 \times 4 \times 8$ to $32 \times 32 \times 64$. The apparent value of τ increases systematically for $L \geq 8$ and is 2.20 ± 0.02 for $L = 32$, which suggests that the exponent for very large systems is the normal percolation value. This is a new test of percolation theory which agrees with Wilkinson's studies on a site-percolation model of drainage [33,34] and on percolation with trapping [31]. This is a significant result, since it indicates that percolation theory can be used to predict quantities which are less easy to measure, such as relative permeability and residual saturation.

3. Relative permeability

We can now write down the results for the relative permeability derived by Wilkinson [33] with some confidence, knowing that percolation theory is likely to give the correct power laws. For $S_{nw} \ll 1$, the nonwetting (invading) fluid's relative permeability is

$$k_{rnw} \sim S_{nw}^{t/\beta}, \quad (4.6)$$

where the exponent t/β is approximately 4.2, while for the wetting fluid

$$k_{rw} \sim (S_{tp} - S_{nw})^{t/(1+\beta)}, \quad (4.7)$$

where $t/(1+\beta) \approx 1.3$ and S_{tp} is the saturation at the terminal point.

D. Measuring relative permeability

We compute relative permeability by finding the hydraulic conductance of the portions of the network occu-

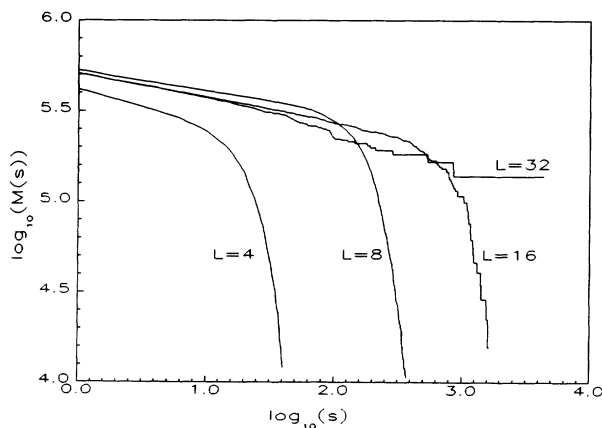


FIG. 5. The cumulant of the trapped-blob-size distribution $M(s)$ against size s for three-dimensional networks $L \times L \times 2L$. The results are the averages of 800 realizations for $L = 8$, 2000 for $L = 8$, 60 for $L = 16$, and 2 for $L = 32$. For $L = 32$, the slope of the curve for intermediate values of s is -0.20 ± 0.02 .

ried by each phase. For a single tube of radius r_t and length l connecting to much wider pore spaces at either end, the conductance, $g = \pi r_t^4 / 8l$ [56,13] if $l \gg r_t$ and the total fluid flow through the tube q for a pressure drop ΔP is $q = g \Delta P / \mu$. We only allow one fluid to flow in a tube. This means that we neglect any contribution to the relative permeability from flow in roughness. We ignore the flow resistance of the pores. We find the overall conductance of the network in the way described in Sec. III. We impose a unit pressure drop across the network and ensure conservation of fluid at each node. The nodal pressures are found using successive over-relaxation [20,57].

There is still some ambiguity associated with nodes filled with one fluid adjoining tubes filled with the other. There can be no flow of nonwetting fluid between tubes separated by a pore filled with wetting fluid. The converse situation is less clear. It is possible for flow in roughness to allow the transport of wetting fluid across pores containing nonwetting fluid. We will compute the relative permeabilities in two limits: (i) We assign a zero conductance to surface wetting films in nodes containing nonwetting fluid. (ii) We assign an infinite conductance to the wetting fluid in all the pores. The realistic situation will be somewhere between the extremes (i) and (ii).

1. Results

Figure 6 shows the drainage relative permeability curves computed on a $16 \times 16 \times 32$ network plotted as a function of pore occupancy fraction. The initial wetting-phase saturation is 100%, as occurs in the initial propagation of oil into a petroleum reservoir (primary drainage). By definition, k_{rw} is normalized to 1 at $S = 1$, where S is the wetting-phase pore occupancy ("saturation"). The tube radii are distributed at random uniformly from 0 to r_{t0} , where r_{t0} is some reference radius. These curves give us the relative permeability for the full range of saturation, outside the limits of validity of Eqs. (4.6)

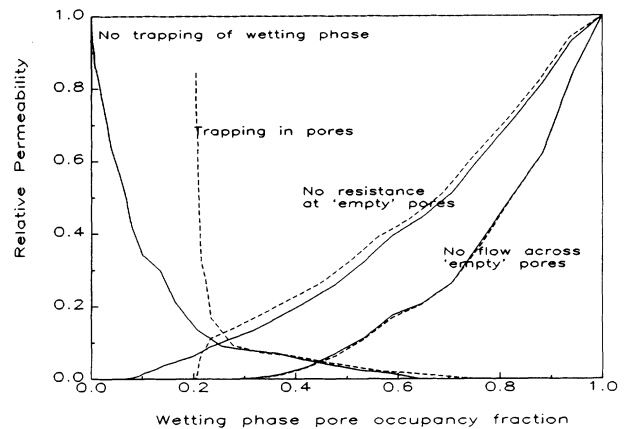


FIG. 6. Drainage relative permeabilities computed on a $16 \times 16 \times 32$ network as a function of pore occupancy. The tube radii are assigned at random uniformly from 0 to r_{t0} . r_{t0} is a reference radius. In this and the subsequent figures for drainage, curves for trapping in pores are indicated by dashed lines. For the wetting phase we assign either no resistance at pores containing nonwetting fluid ("empty" pores), or no flow at "empty" pores.

and (4.7). Within these limits there is qualitative agreement with the percolation results, but our finite-size effects are too large for a good quantitative test of Eqs. (4.6) and (4.7).

Figure 7 shows the same relative permeabilities plotted as a function of tube occupancy fraction. Notice that this significantly alters the shape of the curves compared with Fig. 6, particularly near S_{wi} .

Figure 8 shows relative permeability curves with a wide tube radius distribution: $\log_{10} r_t$ is chosen uniformly from -2 to 2 . The tube radii span four orders of magnitude in size, which represents an extremely heterogeneous rock. In this case the relative permeability rises very quickly as the nonwetting phase tube occupancy increases, since a few wide tubes may carry most of the flow.

With suitable tube and pore radius distribution functions it should be possible to construct curves which lie between the extremes illustrated here and which resemble experimental primary drainage curves. Indeed, percolation network models have successfully matched observed relative permeability curves [13,26]. However, it is not possible to know if these are genuine predictions of relative permeability unless reliable, independent measurements of the rock microstructure have been made. Recent work [58], using a network model representation of a well-characterized random sphere pack, has shown that it is possible to predict drainage relative permeabilities using an invasion percolation model for well-sorted sandstones.

E. Effect of trapping

If there is trapping in both pores and tubes, the wetting-phase relative permeability is the same as if we just have trapping in the pores only, but the permeability of the invading, nonwetting fluid is essentially zero in large systems. This is because the nonwetting fluid is unable to form loops and is thus forced to maintain a tree structure through the system. At breakthrough, percolation theory predicts that for a system of length L , the conductance or permeability is [55] $k_{rnw} \sim L^{-t/\nu}$, where $\nu \approx 0.88$. After breakthrough, if there is trapping in

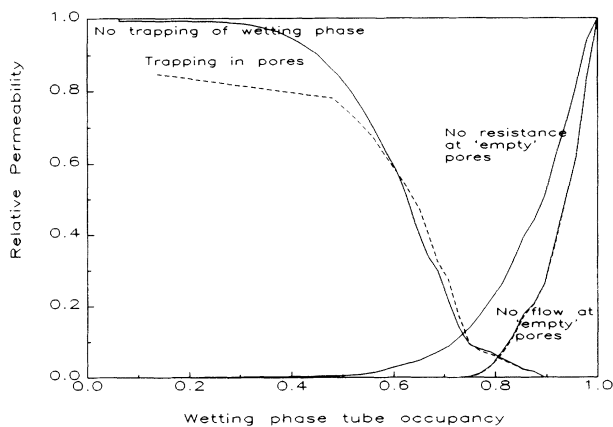


FIG. 7. Drainage relative permeabilities as in Fig. 6, but as a function of tube occupancy.

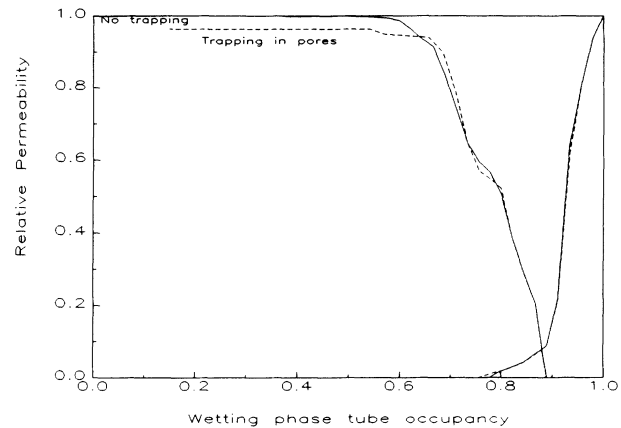


FIG. 8. Drainage relative permeabilities as in Fig. 6, but where the logarithm of the tube radius is distributed at random uniformly from $-2 \ln 10$ to $2 \ln 10$. No resistance at “empty” pores is assumed.

pores and throats, the tenuous pathway of nonwetting fluid which first spanned the network is unable to achieve an appreciably higher conductance by forming loops—almost all the new material forms dead ends, which are branches of the tree structure which do not connect with either the inlet or the outlet faces. This is demonstrated in Fig. 9, where the relative permeability at breakthrough and the terminal points is plotted as a function of system size. The results are averages of 800 realizations for $L=4$, 2000 for $L=8$, 60 for $L=16$, and 2 for $L=32$. The permeability decreases as L^{-2} or faster, and we may predict that the end-point relative permeability, k_{end} obeys $c_1 L^{-2} \geq k_{end} \geq c_2 L^{-t/\nu}$ for constants c_1 and c_2 , which are independent of L , and $t/\nu \approx 2.2$.

This strict trapping rule is only ameliorated by flow in roughness. Thus, if there is no flow along surface grooves, the invading fluid’s relative permeability vanishes in large systems for any saturation. Clearly two-phase flow is possible in porous media, which implies that there must be some flow of wetting fluid in small-scale irregularities.

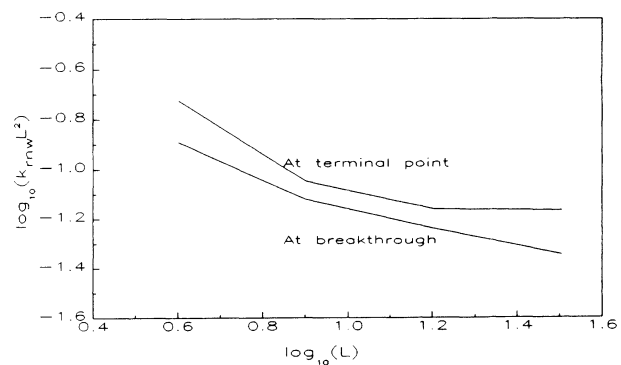


FIG. 9. Nonwetting phase relative permeability k_{rnw} at breakthrough (lower curve) and at the terminal point (upper curve) as a function of system size L for invasion percolation with trapping in both pores and tubes.

The degree of trapping in pores and throats depends on the wettability of the rock, the geometry of the pore space, and the rate at which a drainage experiment is performed. These three effects control the time it takes for the wetting phase to escape from a region completely surrounded by the nonwetting fluid. In an experiment which is done rapidly, and where one phase is only weakly wetting, one expects a low end-point relative permeability and a high value of S_{wi} , whereas for a more strongly wet displaced phase, or if the sample is left for a long time, S_{wi} will decrease to near zero and k_{end} will approach 1.

1. Estimate of the rate of flow in roughness

Imagine that there is wetting fluid in the surface roughness of a throat or tube of radius r_t . Following the approach of Lenormand and Zarcone [22], we model the roughness as an array of small grooves in the pore-grain interface. We assume that these grooves are tiny cylindrical tubes of radius d , spaced a distance $4d$ apart. There are $\pi r_t/2d$ grooves around a tube of radius r_t . The flow through each groove (of length l) is $q_g = (\pi d^4/8l\mu)\Delta P$ and for $\pi r_t/2d$ grooves

$$q = \frac{\pi^2 d^3 r_t}{16l\mu} \Delta P. \quad (4.8)$$

The ratio R of flow in roughness to that through the whole tube is $\pi d^3/2r_t^3$. Typically $d \approx 1 \mu\text{m}$ in throats of radius 10–100 μm , and so $R \sim 10^{-3}$ – 10^{-6} . This small estimate of R allows us to neglect flow in roughness in the calculation of relative permeability. This assertion is confirmed by measurements of the nonwetting phase relative permeability k_{rnw} at the irreducible wetting phase saturation S_{wi} . If flow in roughness is unimportant, $k_{rnw}(S_{wi}) \approx 1$ [59–62].

The time t taken to drain a spherical pore of radius r_v through a single throat containing a wetting film is

$$t = \frac{64\mu r_v^3}{3\pi r_t d^3 \Delta P}. \quad (4.9)$$

Using representative values, $l = 200 \mu\text{m}$, $r_v = 100 \mu\text{m}$, $r_t = 20 \mu\text{m}$, $d = 1 \mu\text{m}$, $\Delta P = 0.1$ – 1 N m^{-2} and $\mu = 10^{-3} \text{ kg m}^{-1} \text{ s}^{-1}$ (the viscosity of water), we find $t \sim 10$ – 100 s . This is the time to drain one pore through a single throat by transport in surface corrugations. The result indicates that in strongly wet systems, flow along surface roughness is sufficiently rapid to remove the wetting phase from many parts of the system during the time that a drainage experiment is performed (1000–100000 s). However, as we have demonstrated, the wetting phase may be trapped in blobs containing tens of thousands of pores for a typical core sample (say $L \approx 100$ – 1000), which would take many hours or days to drain. Thus a relative permeability close to the *trapping in pores* curve may be seen in an experiment, but if the system is allowed to stand for several days, a higher permeability near the *no trapping* curve will be seen. This results in a value of S_{wi} close to zero, which is observed in careful experiments on Berea cores [63–65]. The drainage from single throats will be faster than the result in Eq. (4.9) and so is

unlikely to restrict access of the invading fluid, except if the displaced phase is only partially wetting, or the experiment is very rapid.

F. Capillary pressures

In a low rate drainage experiment, the capillary pressure represents the pressure jump cross the fluid interfaces in the system. In a displacement, this will be determined by the radius of the throat through which the invading fluid front is advancing, Eq. (3.2).

Figures 10 and 11 show the capillary pressure curves for the two networks whose relative permeabilities are shown in Figs. 6 and 8, respectively. Notice that a very broad radius distribution gives a capillary pressure spanning many orders of magnitude, Fig. 11.

The point of inflexion in the capillary pressure curve occurs at breakthrough when the invading phase saturation is very low and given by Eq. (4.1). Breakthrough occurs at the percolation threshold, when $p = p_c$, $r_t = r_c$ in Eq. (4.2). Beyond breakthrough, the capillary pressure may again be described parametrically in terms of an equivalent percolation probability [33]:

$$P_{\text{cap}} - P_{\text{break}} \sim S_{\text{nw}}^{1/\beta} \quad (4.10)$$

when $S_{\text{nw}} \ll 1$. This expression is only valid in a macroscopically homogeneous system, where the saturation increases uniformly everywhere. Notwithstanding finite-size effects, the qualitative agreement between Eq. (4.10) and the simulation results, Fig. 10, is poor.

V. IMBIBITION

We start by describing the microscopic flow mechanisms in imbibition identified in two-dimensional micro-models [3,4,9,14,15,22,27,66–74]. Imbibition cannot be described by a percolation model, since the pore filling is controlled by a cooperative cluster growth mechanism. The process is also intrinsically rate dependent, even when viscous forces are neglected. While these pore scale mechanisms were identified experimentally by Lenormand and Zarcone [22], this study has implemented them in a three-dimensional network model to discuss the implication for relative permeability and capillary pressure.

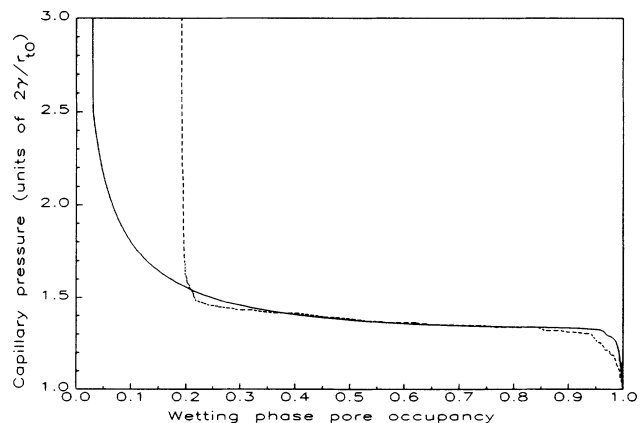


FIG. 10. Capillary pressure curves for drainage with and without trapping in pores.

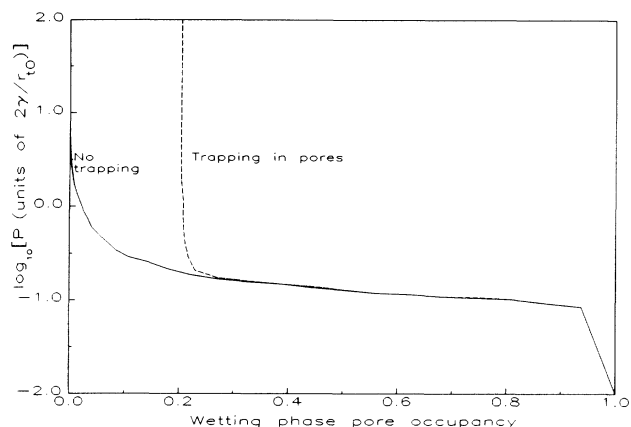


FIG. 11. Capillary pressure curve for the network whose relative permeabilities are shown in Fig. 8.

A. Percolation model for bond filling

A wetting fluid is injected into a material originally full of nonwetting fluid. If the injected fluid is strongly wetting, it will rapidly coat all the pore-grain interfaces with a thin film. As the injection proceeds, this film will swell slowly. Eventually the film will be able to fill the centers of some tubes, starting with the thinnest and progressively filling wider and wider tubes. This “snap-off” or “choke-off” displacement mechanism was originally proposed by Roof [6] and later by Mohanty *et al.* [72,75] and is illustrated schematically in Fig. 12. A displacement involving only “snap-off” is equivalent to a simple bond percolation model. The nonwetting fluid must be able to escape and so a tube cannot become completely full of wetting fluid unless there is a continuous path of nonwetting fluid from that tube to the outlet.

The capillary pressure necessary to fill the tube is [22]

$$P_{cap} = \frac{\gamma}{r_t} \tag{5.1}$$

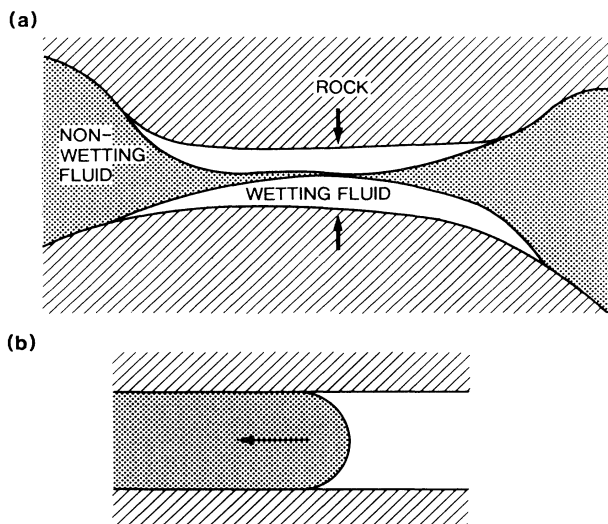


FIG. 12. Displacement processes in imbibition. (a) “Snap-off.” (b) Pistonlike displacement.

for $\theta=180^\circ$ (completely wetting). In imbibition, where the saturation of the wetting phase is increased, processes with the highest capillary pressure are favored. Notice that Eq. (5.1) is a lower pressure than that required to fill a tube of the same radius by a pistonlike displacement, as described in the previous section [$P_{cap}=2\gamma/r_t$ for $\theta=180^\circ$, Eq. (3.2)]. Thus “snap-off” only occurs when a piston displacement is topologically impossible, because there are no pores filled with wetting fluid.

This displacement mechanism is observed experimentally in displacements at very low rate and where the pores are much larger than the tubes connecting them together [22]. Figure 13 shows a two-dimensional pattern at the terminal point. Notice that only tubes are filled—if all the pores are wider than any of the tubes, the pores are filled last, by which time the nonwetting fluid is trapped and no further displacement is possible.

General results from percolation theory can be used to predict the behavior near breakthrough, now that we know trapping does not affect the percolation exponents (see Sec. IV). The results come from ordinary percolation theory once the change in tube occupancy ΔF_t is identified with changes in the effective percolation probability Δp [33,54]:

$$k_{rw} \sim (F_t - F_{tc})^t \tag{5.2}$$

if $F_t - F_{tc} \ll 1$, where $t \approx 1.9$ and F_{tc} is the tube occupancy at breakthrough. The pore occupancy is always zero. Also,

$$P_{break} - P_{cap} \sim F_t - F_{tc} \tag{5.3}$$

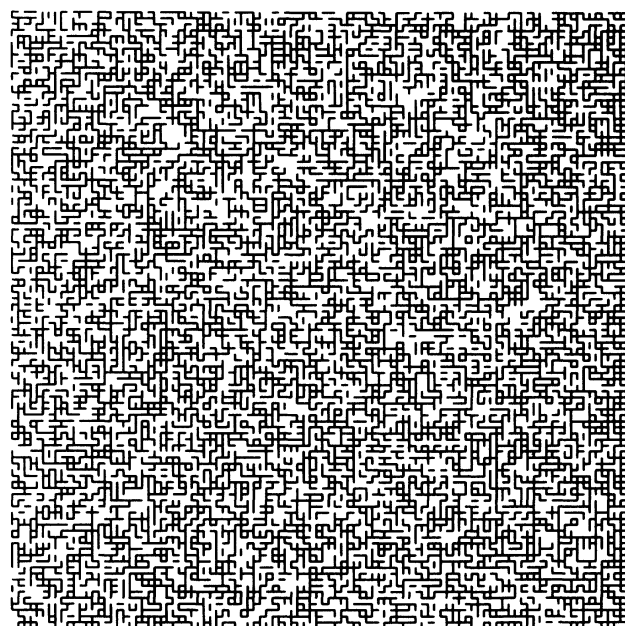


FIG. 13. Imbibition by “snap-off” computed on a 100×100 square grid at the terminal point.

B. Pore filling

Lenormand and Zarcone have observed and investigated a variety of pore- and tube-filling mechanisms in imbibition [22] and have calculated capillary pressures in a square grid of tubes and pores. Figure 14 illustrates how a pore may be filled when one or more of its surrounding tubes are full of wetting fluid. Since there is likely to be a thick film of wetting fluid in the pore in these circumstances, the radius of the fluid interface will be considerably less than r_v , the pore radius, which allows even large spaces to fill with wetting fluid. For a lattice of coordination number z , there are $z - 1$ such imbibition mechanisms (called I_1 to I_{z-1}), which represent filling of a pore when 1 to $z - 1$ connecting tubes contain nonwetting fluid. The capillary pressures are ranked $P_{cap}(I_{z-1}) < \dots < P_{cap}(I_2) < P_{cap}(I_1)$. The I_z mechanism is topologically impossible because at least one of the attached throats must be occupied by wetting fluid.

We can reproduce the extremes of the experimental behavior. Lenormand and Zarcone [22] found that in a network with pores which were only slightly larger than the tubes, the I_1 and I_2 mechanisms had the highest capillary pressures and the displacement was a type of random cluster growth process. In real materials, this type of displacement is unlikely to be seen, since large pores would prevent such clusters growing appreciably. If the pores were much larger than the tubes, then none of the pores filled and we saw the bond percolation picture described earlier. For medium-sized pores, the imbibition was controlled by tube filling ("snap-off") and I_1 . Thus pores only filled when all but one of the surrounding tubes were full.

This mixed pore-tube filling process may be simulated numerically. We generate a network as before, with ran-

domly assigned tube radii, and pores all of the same size. The tubes are filled one at a time, starting with the thinnest and then the next thinnest and so on. At any stage in the simulation, if an empty pore has $z - 1$ (3 in two dimensions and 5 in three dimensions for square and cubic grids, respectively) tubes connected to it which are filled with wetting fluid, the pore and the last empty tube are filled. However, we only fill a tube or pore if the displaced nonwetting fluid can escape to the outlet. Figure 15 shows a two-dimensional displacement at the terminal point. At breakthrough in three dimensions, very few of the pores are filled, but many more are filled eventually, and often form large connected clusters.

C. No film flow or high rates

In the models above we have assumed that slow flow along thin films is sufficient to supply wetting fluid to all parts of the network. If we inject at a high rate, or if there is no wetting film, this will not be possible and the displacement may only proceed by a pistonlike mechanism, with a connected advance of fluid through the centers of the tubes, as in drainage, which has been described by Lenormand and Zarone [22] and is illustrated in Fig. 16. On a square lattice the displacement is a succession of I_3 and I_2 events. Topological constraints require an I_3 even before I_2 is possible, although I_2 is favored since it has the higher capillary pressure.

1. Estimate of the extent of film flow

Figure 17 is a schematic illustration of the advance of a wetting fluid at intermediate flow rates. Near the inlet the nonwetting fluid is displaced by pistonlike movement from tubes and by the I_1 mechanism from pores. In advance of this, film flow along microscopic roughness al-

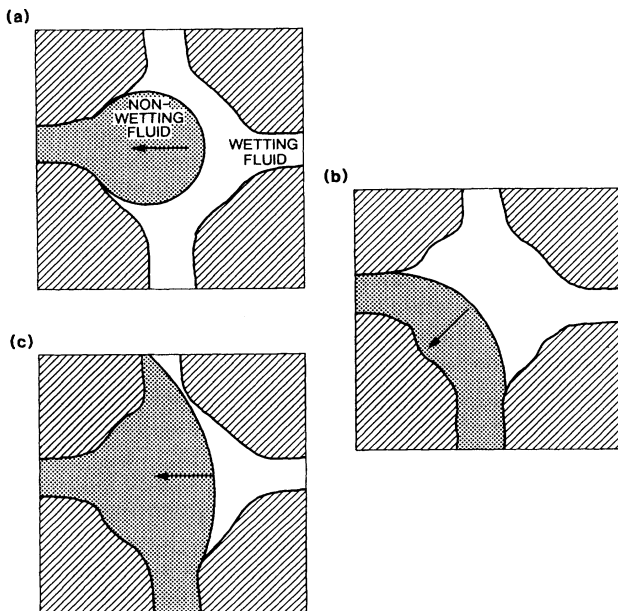


FIG. 14. Mechanisms of pore filling in imbibition in a four-fold-coordinated lattice. (a) I_1 . (b) I_2 . (c) I_3 . I_4 is not possible if the pores are larger than the throats.

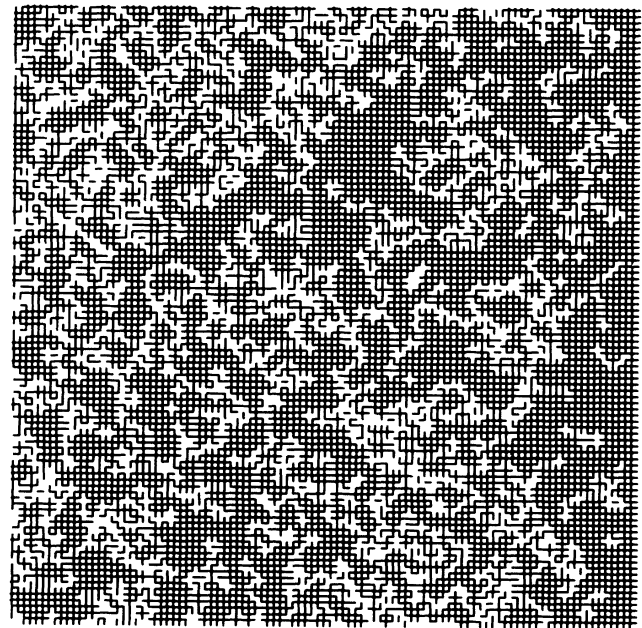


FIG. 15. Imbibition by "snap-off" and I_1 on a 100×100 square grid at the terminal point.

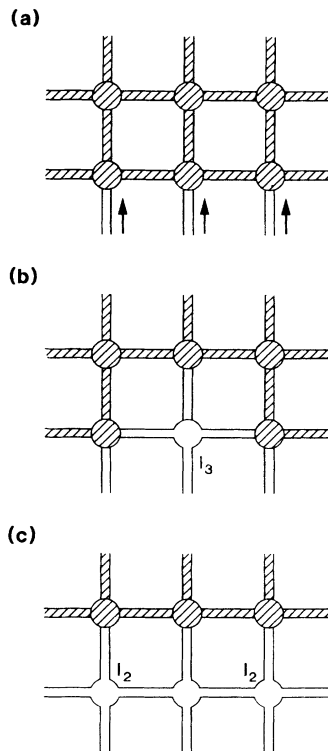


FIG. 16. Frontal advance in imbibition. (a) The first layer of thin tubes is filled with wetting fluid. (b) By I_3 , one pore and the adjoining tubes are filled. (c) By I_2 the remaining pores in the first layer are filled and the displacement proceeds as from (a), but one layer up.

lows some tubes to be filled by “snap-off.” Beyond this region is a wide, advancing edge of the wetting film.

We assume that the capillary pressure rises linearly from a value $P_{\text{cap}}(I_1)$ at a distance l_1 from the inlet (the limit of the “frontal advance”) to $2\gamma/d$ at l_2 . (For simplicity we take $\theta=180^\circ$ in this treatment.) Furthermore, we consider the pore space to be a bundle of parallel and nonintersecting capillary tubes with radius r_t and ignore tube filling in the region l_1 to l_2 . Following the argument of Lenormand and Zarcone [22] we find, for constant flow rate,

$$l_2 = l_0(1 - e^{-l_2/l_0}) + \frac{q_0 t}{\pi r_t^2}, \quad (5.4)$$

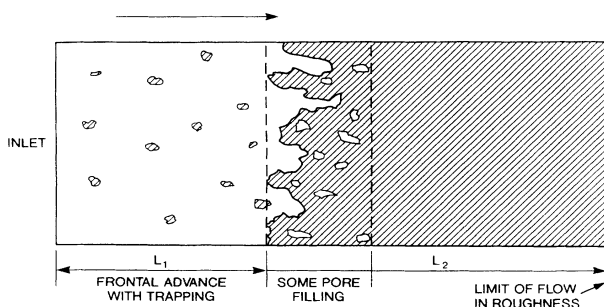


FIG. 17. The advance of a wetting fluid at intermediate flow rates.

where

$$l_0 = \frac{\pi \gamma r_t^2 d}{4 \mu q_0} \quad (5.5)$$

and $l_2=0$ when $t=0$.

The width of the thin film in advance of the connected front is $l_2 - l_1$:

$$l_2 - l_1 \approx l_0(1 - e^{-l_2/l_0}). \quad (5.6)$$

At long times, when $l_2 \gg l_0$, $l_2 - l_1 = l_0$. l_0 may be rewritten in terms of a capillary number C_A , which is the ratio of the viscous pressure drop to the capillary pressure drop in a typical tube in the network:

$$C_A = \frac{\Delta P_{\text{visc}}}{\Delta P_{\text{cap}}}, \quad (5.7)$$

where ΔP_{cap} is given by Eq. (3.2) and, for Poiseuille flow, Eq. (3.1), $\Delta P_{\text{visc}} = 8\mu l q_0 / \pi r_t^4$. Thus

$$C_A = \frac{4\mu l q_0}{\pi \gamma r_t^3} \quad (5.8)$$

for $\theta=180^\circ$, and so

$$l_0 = \frac{dl}{C_A r_t}. \quad (5.9)$$

In the micromodel experiments of Lenormand *et al.*, the capillary number C_A varied from 10^{-4} , which gave a flat frontal advance to 10^{-8} for which a bond percolation displacement controlled by “snap-off” was observed. These capillary numbers are also typical of the range in oil reservoirs. For small scale roughness, one would expect the ratio d/r_t to be approximately 10^{-4} – 10^{-1} , which means that l_0 is in the range 1 – 10^7 pore-throat lengths. When l_0 is only of the order of l , there is essentially no wetting film and the displacement proceeds along a connected front, whereas for the lower rates, the film quickly permeates the whole system and a disconnected displacement front is seen. It is more usual experimentally for the wetting phase to be hydraulically connected by thin films or in microscale crevices [64,66,76,77].

We have not explicitly considered the width of the region where a connected pathway of tubes filled by “snap-off” exists just in advance of the connected front. In this region, the exact configuration of the filled tubes affects the local pressure gradients, which in turn influences how the displacement progresses. In Sec. VI we will consider this problem and show that the width of this layer, l_t , scales as a fractional power of C_A : $l_t \sim l C_A^{-f}$, where $f=0.49$. This means that for very low C_A , l_t is much smaller than l_0 , and even for extremely slow flow is only about 100–1000 pore-throat lengths.

It is possible to simulate imbibition at an intermediate flow rate in a network with a distribution of both pore and throat radii. A simple but crude procedure is to impose a capillary pressure gradient across the network. The capillary pressure increases linearly from inlet to outlet. We start with a very high capillary pressure at

the inlet and lower this pressure as the displacement proceeds. Pore- and throat-filling processes which have the highest capillary pressures are favored and will occur, if topologically possible, when the imposed pressure drops below the capillary pressure for the process. Only tube filling is allowed at large distances from the outlet, but I_1 , I_2 , and I_3 may be possible near the inlet. We can specify a pore-radius distribution which assigns different capillary pressures for pore filling. Figure 18 shows an imbibition on a 100×100 network and represents a displacement at a capillary number of approximately $0.01d/r_t$ such that l_0 is about 100 tube lengths. A linear pressure gradient is imposed across the system and the pore radii are chosen such that in Fig. 18, 5% of the nodes can fill by I_3 and 20% by I_2 near the inlet. Where the wetting film has penetrated there is some tube and pore filling in advance of a ragged connection interface. The regions which the wetting fluid has swept resemble Fig. 15, which simulated a much lower rate advance.

D. Results

Figure 19 shows computed relative permeability curves as a function of tube occupancy on a $16 \times 16 \times 32$ network with the tube radii distributed uniformly from 0 to r_{t0} for the bond percolation model, and for the mixed bond-pore mechanism. We have assigned an infinite conductance to the wetting fluid in all the pores.

The percolation theory relation, Eq. (5.2), is tested in Fig. 20, where k_{ri} is plotted as a function $F_t - F_{tc}$ on dou-

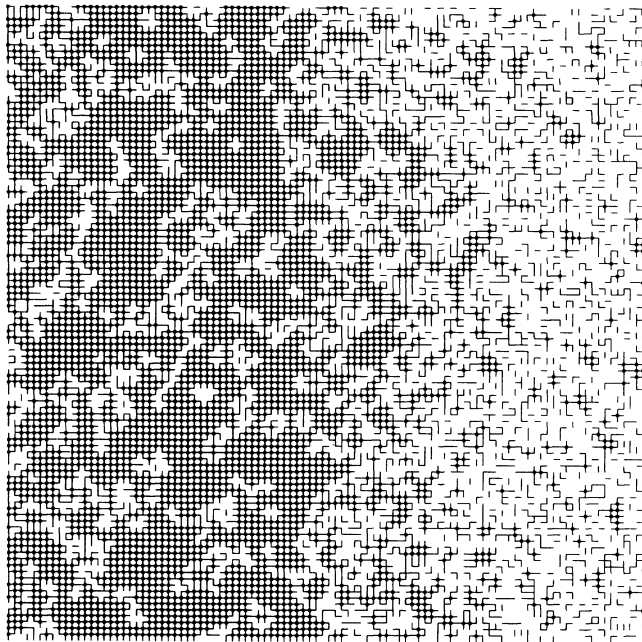


FIG. 18. Imbibition at intermediate capillary number on a 100×100 square network. Pores and tubes completely filled by injected fluid are shown. The width of the advancing wetting film (which is not shown) is approximately 100 tube lengths. We see a ragged frontal advance near the inlet, preceded by some pore and tube filling, where the fluid is supplied by film flow.

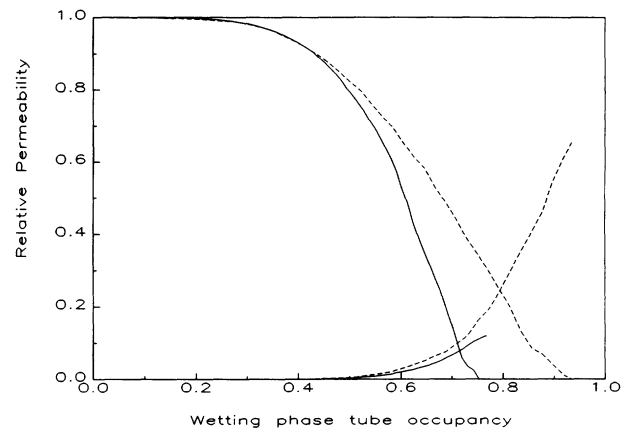


FIG. 19. Imbibition relative permeabilities as a function of tube occupancy on a $16 \times 16 \times 32$ network. Solid lines—the bond percolation model, “snap-off.” Dashed lines—displacement by “snap-off” and I_1 .

bly logarithmic axes for the bond percolation model and for imbibition by “snap-off” and I_1 . The agreement between the theory and the numerical results is poor because the networks we use are fairly small, but the data are consistent with an approximately power-law regime at very small relative permeability.

Figure 21 plots capillary pressure curves. P_{cap} is defined by Eq. (5.1), where r is the largest tube to be filled in the network.

Film flow, or flow along microscopic roughness, makes a negligible contribution to the overall wetting phase saturation, or directly to the relative permeability. However, it does influence the nature of the pore scale displacement and hence the fluid configuration. This in turn does affect the relative permeability.

We have not computed relative permeabilities for an intermediate rate imbibition, illustrated in Fig. 18. The mean saturation varies across the network. In order to compute $k_r(S)$ we need to find the flow conductivity in a

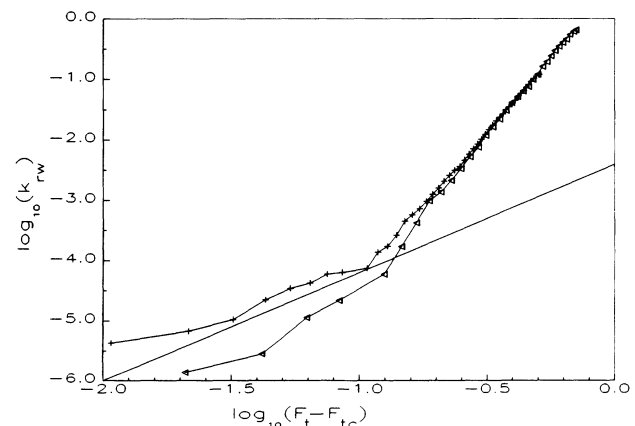


FIG. 20. Imbibition relative permeabilities. $\log_{10}k_{rw}$ is plotted against $\log_{10}(F_t - F_{tc})$. Crosses, “snap-off” only. Triangles, “snap-off” and I_1 . The solid line is the prediction from percolation theory.

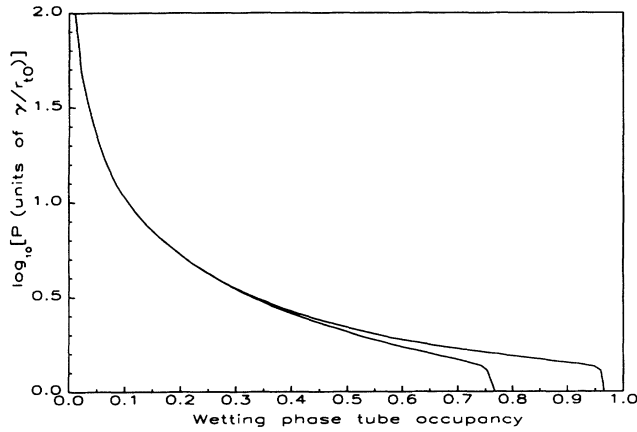


FIG. 21. Capillary pressures as a function of tube occupancy. Lower curve, “snap-off.” Higher curve, “snap-off” and I_1 .

region where the saturation is locally homogeneous, which we cannot do reliably in our relatively small three-dimensional simulations. This point will be discussed further in the next section and explains why later we will not attempt to find the relative permeability in inhomogeneous displacements with gravity.

VI. GRAVITATIONAL AND VISCOUS FORCES

Our treatment has so far only considered displacements at very low flow rates and has ignored the effects of gravity and viscous forces. We will use a combination of percolation theory and network modeling to predict how the overall displacement pattern is affected by these forces. The arguments using percolation theory will follow the approach of Wilkinson [33,34,78]. The effect of gravity on drainage has been explored numerically and experimentally by Jøssang [79] and Birovljev *et al.* [80], while the influence of high flow rates on drainage relative permeabilities has been investigated by Blunt and King [19,20]. The aim of this section is to quantify the perturbative influence of viscous and buoyancy forces on relative permeability and to show why relative permeability is still a robust concept even when the large-scale behavior of the flow is no longer solely controlled by capillary forces.

A. Correlation lengths and finite-size effects

The results from percolation theory have assumed that the displacements occur in an infinitely large system, whereas our numerical results were computed on finite-sized networks (16 pores across or larger); experiments on core samples a few inches long are typically 1000 pores across. This affects the saturations at which breakthrough and the terminal point occur. In drainage, using an invasion percolation model, we showed that for a system of size $L = \xi$, the saturation at breakthrough $S_{\text{break}} \sim \xi^{D-d}$ [Eq. (4.1)]. The exponent is approximately -0.5 , which indicates that for $\xi = 16-32$ (our simulations) S_{break} may be of the order 10–25%. Even for an experimental core sample ($\xi \approx 1000$) breakthrough may only occur at a saturation of around 5%, while in an effectively infinite reservoir, there is a connected pathway

of nonwetting fluid at virtually a zero saturation. This is the reason why we did not test the theoretical relations (4.6) and (4.7) numerically—our finite-size effects are too large for any reliable determination of exponents to be made.

We will carefully consider the finite-size effects on saturation for two important reasons: (1) we are only able to perform simulations on networks which represent much smaller systems than experimental core samples, (2) finite-size percolation will be advanced as the model to determine the effects of buoyancy on residual saturation.

In the finite-sized system the apparent percolation threshold p_c is decreased. The apparent percolation probability for a system of length ξ is [54]

$$p_{\text{eff}} - p_c \sim -\xi^{-1/\nu}. \quad (6.1)$$

The exponent $1/\nu$ is approximately 1.2. In our simulations of a bond percolation model of imbibition the shift in p_c was typically only 1–2%. This means that our estimate of the saturation (bond occupancy) at breakthrough was more accurate than for drainage.

A finite-sized system affects the distribution of (trapped) cluster sizes at p_c , where p_c now represents the percolation threshold of the defending fluid. $N(s) \sim s^{-\tau}$ is modified by a scaling function which introduces a cutoff at $s \geq s_{\text{max}}$, where $s_{\text{max}} \sim \xi^D$,

$$N(s, \xi) \sim s^{-\tau} G(s/s_{\text{max}}). \quad (6.2)$$

If we naively assume $G(x)$ is a step function [$G(x) = G(0)$, $x \leq 1$, $G(x) = 0$, $x > 1$], then the change in saturation ΔS , is due to finite size, is (defining “saturation” for this argument to be the pore occupancy of the defending phase)

$$\sum_{s=s_{\text{max}}}^{\infty} sN(s) \sim s_{\text{max}}^{2-\tau} \int_1^{\infty} x^{-(\tau-1)} dx \sim \xi^{-\beta/\nu} \quad (6.3)$$

using the scaling relation $D(2-\tau) = -\beta/\nu$ (cf. Appendix in Ref. [31]). However, we will illustrate that the change ΔS is more subtle.

One can determine $N(s, \xi)$ by considering an infinite system at $p \approx p_c$ and dividing it into cubes of side ξ . The average number of the truncated parts of the largest clusters as well as the distribution of smaller clusters in the cubes is $N(s, \xi)$. The change in the trapped saturation at p_c is

$$\Delta S \equiv S(\infty) - S(\xi) = \sum_{s=1}^{\infty} s [N(s) - N(s, \xi)]. \quad (6.4)$$

However, by the construction of $N(s, \xi)$ this sum over the cluster sizes must be zero (the “mass” has simply been redistributed) [31].

In general $N(s, \xi; p) [= s^{-\tau} G(s/s_{\text{max}}; p)]$ is a function of p and the trapped saturation for a finite system is determined at p_{eff} . Thus

$$\begin{aligned} \Delta S_{\text{eff}} &= \sum_{s=1}^{\infty} s [N(s) - N(s, \xi; p_{\text{eff}})] \\ &\sim s_{\text{max}}^{2-\tau} \int_0^{\infty} x^{1-\tau} [(G(0) - G(x; p_{\text{eff}}))] dx. \end{aligned} \quad (6.5)$$

If we expand $G(x; p_{\text{eff}}) \approx G(x) + (p_{\text{eff}} - p_c)G'(x)$ and use Eq. (6.1) and the scaling relation in Eq. (6.3) we obtain

$$\Delta S_{\text{eff}} \sim \xi^{-(\beta+1)/\nu}. \quad (6.6)$$

This scaling relation was first derived by Wilkinson [33] using a different expression for ΔS . Here we have stressed that the change in saturation is due to the shift in the cluster size distribution for a finite system from its form at p_c to that at p_{eff} .

B. Buoyancy forces

Buoyancy and viscous forces introduce a finite correlation length even in an infinite system. We will assume that the effects on ΔS of this correlation length is the same as introduced by a finite-size system. We now need to determine a correlation length due to the buoyancy force, insert this relation for ξ in Eq. (6.6), and compare with our simulation results to check this assumption *a posteriori*.

Consider a drainage experiment where light, nonwetting oil is injected at the top of a piece of rock containing heavier, wetting water. The density difference between the fluids means that the oil preferentially resides at the top of the sample and the water at the bottom. Thus it requires a greater pressure to force the oil through a throat near the bottom of the sample than near the top. Although the interfacial tension between the fluids is usually large, which means that capillary forces are significant, the density difference may also be high and so gravitational effects may be apparent in tall samples.

There is now an entry pressure P_{entry} for each throat which is a sum of the capillary and gravitational pressures:

$$P_{\text{entry}} = -\frac{2\gamma \cos\theta}{r_t} - \delta\rho gh, \quad (6.7)$$

where h is the height of the throat (defining $h=0$ as the top of the sample) and $\delta\rho$ is the difference between the density of the wetting phase and the density of the nonwetting phase. The relative importance of capillary to buoyancy forces is defined by a bond number B , where

$$B = -\frac{\delta\rho g r_{t0} l}{2\gamma \cos\theta}. \quad (6.8)$$

B represents the ratio of the buoyancy pressure in a single tube of height l ($\delta\rho gl$) to a typical capillary pressure in a throat $-2\gamma \cos\theta/r_{t0}$. The surface tension γ of water in contact with air is 0.07 N m^{-1} [81]. In contact with most oils, γ is typically around half this value, say 0.04 N m^{-1} . The density difference $\delta\rho$ may vary from a maximum of 1000 kg m^{-3} (water and gas) to as low as 100 kg m^{-3} —let us take a value of 500 kg m^{-3} for an estimate of B . Then for $\theta=180^\circ$, $l=100 \mu\text{m}$ and $r_t=20 \mu\text{m}$, $B \sim 10^{-4}$, which is very small and indicates that at the microscopic level the effect of buoyancy forces is negligible. However, in a large sample the total gravitational pressure may be comparable to the capillary pressure. Consider a sample N_z pores high, then a global bond number which represents a ratio of the gravitational pressure across the whole sample to a typical capillary pressure is $N_z B$. If

the system is, for instance, 10 cm across, then N_z will be of the order of 1000 and so $N_z B \approx 0.1$.

1. Percolation theory

Capillary flows with gravity have been studied theoretically by Wilkinson [33,34] and experimentally by Jossang [79] and Birovljev *et al.* [80]. The displacements resemble those predicted by the invasion percolation model, but there is a maximum correlation length in the system, which represents the linear extent of the largest regions which are ever enclosed by injected fluid. Equation (6.7) indicates that the proportion of tubes which can be accessed at a given injection pressure increases with height h . It is as though the effective percolation probability varies linearly with h . The buoyancy force will affect the most extended clusters and truncate $N(s)$ in a way analogous to percolation in a finite-sized system. The key consequence for ΔS of introducing ξ , as discussed above, is to cause a shift in $N(s; \xi; p)$ over the interval δp_{eff} between p_c and p_{eff} . To be able to resolve this shift, the variation in the percolation probability δp over the largest cluster, $\delta p \approx \xi_B B$, must not be larger than δp_{eff} : $\xi_B B < \delta p_{\text{eff}} \sim \xi_B^{-1/\nu}$, or the maximum ξ_B scales as [33]

$$\xi_B \sim B^{-\nu/(1+\nu)}. \quad (6.9)$$

The value of ν in three dimensions is 0.88 and for the bond number calculated above $\xi_B \approx 100$ nodes (measured in units of bond length l) instead of the result 10^4 nodes based on the naive dependence $\xi_B \sim 1/B$. Viewed on length scales less than $\xi_B l$, the displacement resembles one modeled by invasion percolation without gravity, while the effects of gravity are noticed for samples taller than $\xi_B l$, which in this example represents a height of approximately 1 cm.

The decrease in residual saturation is [33]

$$S_{\text{wi}}(B=0) - S_{\text{wi}}(B) \sim B^{(1+\beta)/(1+\nu)}, \quad (6.10)$$

where the exponent $(1+\beta)/(1+\nu)$ is approximately 0.77. Equation (6.10) predicts a decrease in S_{wi} of between about 0.1% to 1% in most oil reservoirs, compared with displacements with fluids of matched density.

2. Network simulations

We can demonstrate the effect of buoyancy forces using the network model. The simulation is identical to that presented in Sec. IV, except that instead of filling available tubes in order of radii, we fill in order of an entry pressure P given by Eq. (6.7). The height h is considered to be the height of the middle of the tube.

Figures 22 and 23 illustrate two-dimensional displacements at the terminal pint for drainage and the ‘‘snap-off’’ and I_1 model of imbibition, respectively. The bond number is 0.001 in Fig. 22, giving a correlation length ξ_B of approximately 30 pore-throat lengths, or one-tenth of the system size. This can be verified by noting that the largest trapped blobs of displaced phase are approximately 30 pore sizes across. Figure 24 shows the cumulant of the distribution of trapped blobs in a three-dimensional network for drainage at the terminal point, $M(s)$ [see

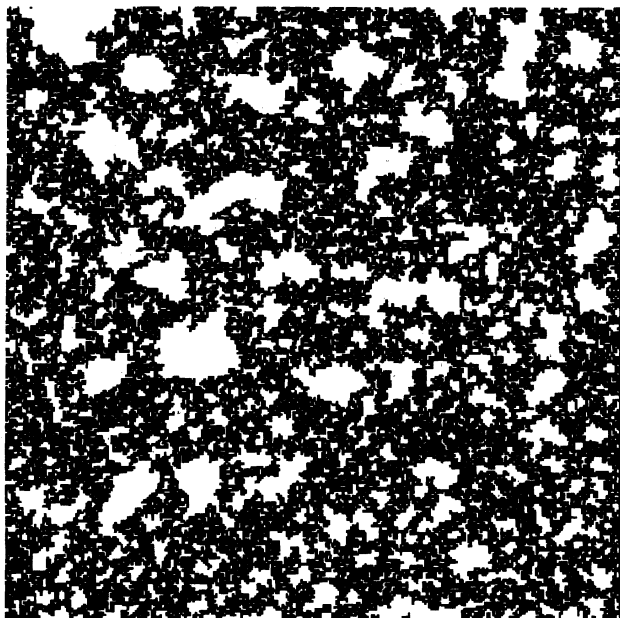


FIG. 22. Drainage under gravity with trapping at a bond number $B=0.001$ simulated on a 300×300 square lattice, shown at the terminal point.

Sec. IV and Eq. (4.5)] for various values of B . Figure 5 showed $M(s)$ for lattices of different size. Notice that $M(s)$ on a large lattice with gravity resembles that for $B=0$ on a smaller lattice. However, a comparison of Figs. 5 and 26 indicates that using Eq. (6.9) systematically overestimates the apparent correlation length, and that this effect is most marked for the larger values of ξ_B .

The simulations are performed on a finite-sized lattice

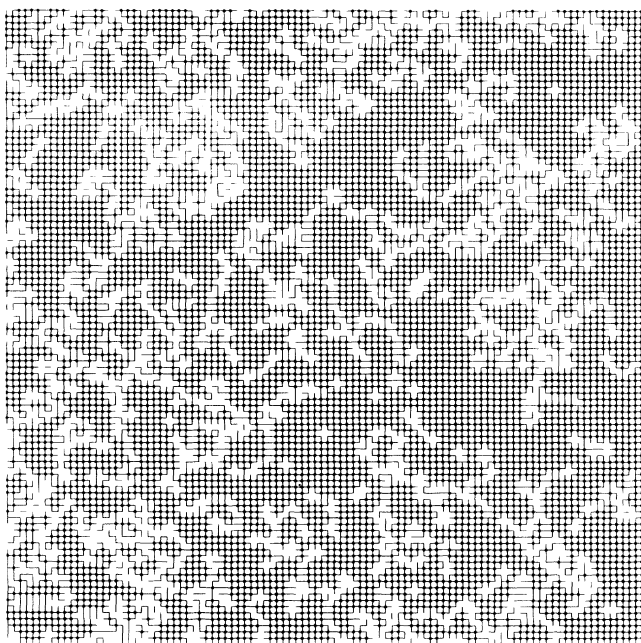


FIG. 23. Imbibition by “snap-off” and I_1 under gravity with a bond number $B=0.02$ simulated on a 100×100 square lattice, shown at the terminal point.

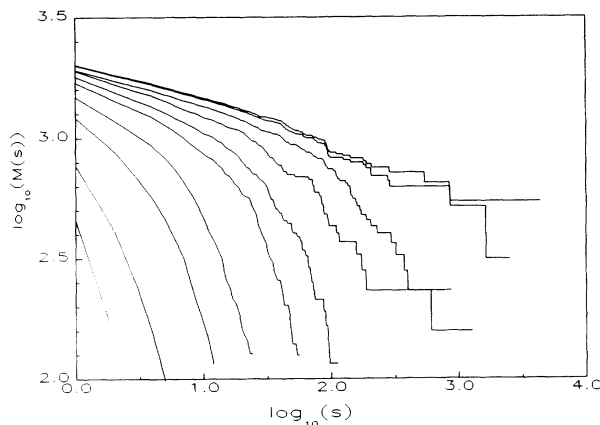


FIG. 24. The cumulant of the trapped-blob-size distribution function $M(s)$ against blob size s on $32 \times 32 \times 64$ lattices for various values of the bond number B . From left to right the curves have a buoyancy correlation length ξ_B from Eq. (6.9) of 1.5, 2, 3, 4, 6, 8, 12, 16, 32, and ∞ .

with $L=32$. We postulate an effective correlation length, which is a combination of contributions from both the lattice size and B :

$$\frac{1}{\xi} = \frac{1}{L} + \frac{1}{\xi_B}, \tag{6.11}$$

where ξ_B is the buoyancy correlation length, Eq. (6.9).

Figure 25 shows the trapped pore occupancy (“saturation S ”) as a function of $1/\xi$ from Eq. (6.11) for both drainage with trapping in pores and the “snap-off” and I_1 model of imbibition. This graph is used to estimate the saturation when $\xi=\infty$ so that we can compute $\Delta S=S(\infty)-S(\xi)$, which is shown in Fig. 26. The straight line in the figure has the theoretical slope $-(\beta+1)/\nu$, Eq. (6.6) —for both drainage and imbibition the change in residual saturation is consistent with finite-size percolation theory. The concept of a finite correlation length can now be extended to viscous forces, where we

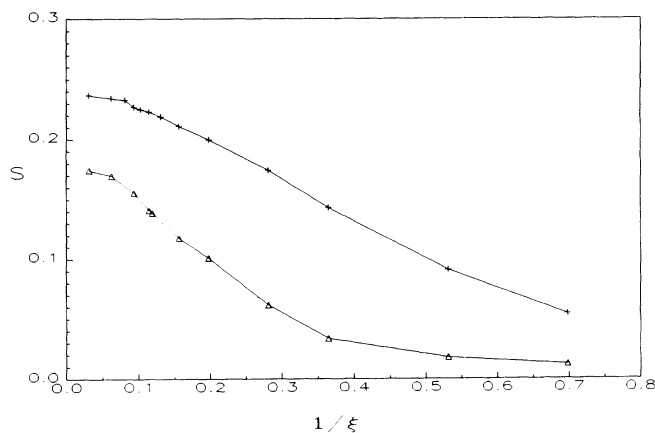


FIG. 25. Trapped saturation S (pore occupancy) as a function of effective correlation length ξ for drainage with trapping (crosses) and the “snap-off” and I_1 model of imbibition (triangles).

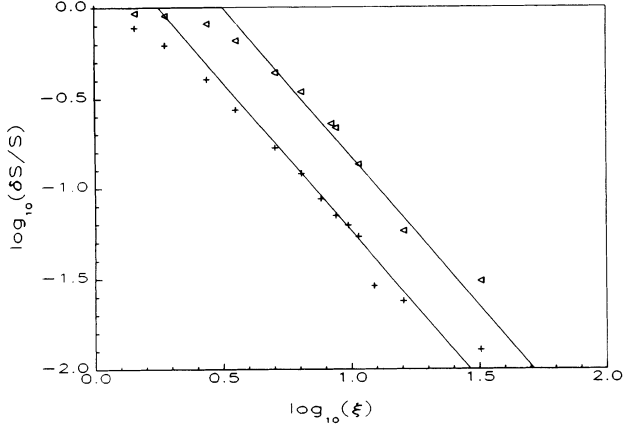


FIG. 26. Fractional decrease in trapped phase pore occupancy $\Delta S/S$ on a $32 \times 32 \times 64$ network for drainage (crosses) and imbibition (triangles) for different correlation lengths ξ . The straight line is the prediction from percolation theory with a slope given by Eq. (6.9).

are unable to perform reliable simulations to verify our predictions.

C. Rate-dependent effects

The key idea of the previous section is to consider a box of length equal to the correlation length ξ , which is determined self-consistently by comparing the shift in p_c induced by the box with the variation in P_{cap} across the largest cluster caused by a perturbative force. We apply this approach directly to viscous forces by imagining the initial entry of nonwetting fluid through a unit area of material across a distance x (measured in units of a typical tube length l .) We will consider the nonwetting phase to be at breakthrough and choose x to be the correlation length. We impose a flux Q_{nw} through the nonwetting phase and a flux Q_w through the other, which is not at threshold and consequently is well connected. The permeability of each phase is defined by

$$Q_w = \frac{K_w}{\mu_w} \frac{\Delta P_w}{xl} \quad (6.12)$$

and

$$Q_{\text{nw}} = \frac{K_{\text{nw}}}{\mu_{\text{nw}}} \frac{\Delta P_{\text{nw}}}{xl}. \quad (6.13)$$

The permeability of the wetting phase will be of the same magnitude as the permeability with just a single phase present, K , which for an array of tubes of radius r_t is $\pi r_t^4/8l^2$. However, in a percolation model, the permeability of the portion of the medium occupied by a phase at breakthrough (or at the terminal point) is much lower, because it only occupies a very wispy path through the network. We shall assume that we may use percolation theory to calculate the permeability (which is equivalent to the conductance) at the percolation threshold:

$$K_{\text{nw}} \approx Kx^{-t/\nu}, \quad (6.14)$$

where t/ν is approximately 2.2 in three dimensions [33].

Notice that K in Eq. (6.14) scales with a negative power of x . Then the pressure drops across the two phases are

$$\Delta P_w = \frac{Q_w l \mu_w}{K} x \quad (6.15)$$

and

$$\Delta P_{\text{nw}} = \frac{Q_{\text{nw}} l \mu_{\text{nw}}}{K} x^{t/\nu+1}. \quad (6.16)$$

The pressure drops give an estimate for the change in P_{cap} across a cluster, which is equivalent to a change in allowed fraction p . If we assume that the pressure drop in the nonwetting phase is greater than, or of the same order as, the pressure drop in the wetting phase, we may write

$$\delta p_c \sim -C_{\text{nw}} x^{t/\nu+1}, \quad (6.17)$$

with capillary number C_{nw} given by

$$C_{\text{nw}} = -\frac{4l\mu_{\text{nw}}Q_{\text{nw}}}{\pi\gamma \cos\theta r_t^3}. \quad (6.18)$$

We now set $x = \xi V$, the viscous correlation length and assert that the shift in allowed fraction, Eq. (6.17), must be less than the shift in p_c , $\delta p \sim \xi_V^{-1/\nu}$, to be able to have a finite-size percolation cluster distribution of the invader phase, i.e., $C_{\text{nw}} \xi_V^{t/\nu-1} < \delta p \sim \xi_V^{-1/\nu}$ or the maximum ξ_V scales as [82]

$$\xi_V \sim C_{\text{nw}}^{-\nu/(t+\nu+1)}, \quad (6.19)$$

where the exponent is approximately -0.23 . Viewed on scales less than ξ_V , the displacement resembles an infinitesimal flow rate, while the effects of viscous forces are evident for $x > \xi_V$.

We may also consider the trapping of the nonwetting phase in imbibition. In this case the nonwetting phase is at its terminal point. The analysis above follows, since the wetting phase is still well connected and the permeability of the nonwetting phase still resembles a percolation cluster. For drainage it is natural to write the correlation length in terms of the flux of nonwetting fluid. However, for trapping in imbibition, the displacement is controlled by the flow of wetting fluid and it is more natural to write ξ_V in terms of Q_w , assuming that the pressure drop in the wetting phase is of the same order of magnitude or greater than the pressure drop in the nonwetting phase. Then we may follow the analysis above to find

$$\delta p_c \sim -C_w x, \quad (6.20)$$

where

$$C_w = -\frac{4l\mu_w Q_w}{\pi\gamma \cos\theta r_t^3}. \quad (6.21)$$

The effective percolation probability p now varies linearly with x , as it did for buoyancy forces, and so we find

$$\xi_V \sim C_w^{-\nu/(1+\nu)} \quad (6.22)$$

as derived by Wilkinson [33]. The exponent $\nu/1+\nu$ is

approximately 0.49. Equation (6.6) may be used to calculate the shift in residual saturation which scales with C_w with the same exponent, $(1+\beta)/(1+\nu) \approx 0.77$ as it does for bond number B , Eq. (6.10).

We may consider a steady-state experiment where both phases are injected through a system to achieve a homogeneous saturation distribution and the pressure drops sustained by both fluids are the same. Fluctuations in the local pressure give capillary pressure differences that are of the same order of magnitude as either of the pressure drops Eqs. (6.15) or (6.16). Thus the viscous correlation length may be written as a function of either capillary number. The different exponents in Eqs. (6.19) and (6.22) are explained by the very different fluxes, which are in the ratio of the permeabilities of each phase: $Q_w/Q_{nw} = C_w/C_{nw} = K_w/K_{nw} = \xi_V^{t/\nu}$. If we define the correlation length as a function of the flux of the more mobile phase, the effect of viscous forces is similar to that of buoyancy, and we see a typical ξ_V in the range 100–1000 tube lengths. The important point is that with either choice of pressure drop, Eq. (6.15) or (6.16), the resulting correlation length must be approximately the same in this case.

D. Meaning of a correlation length

In our discussion on the meaning of relative permeability, Sec. III, we mentioned that k_r was only a well-defined, intensive property of the flow when the length over which it was measured was much larger than any physical correlation length in the system. For very low rate drainage or imbibition, the viscous correlation length is effectively finite. This means that the saturation at breakthrough and the relative permeability near the end points is a systematic function of the size of the system L in which the measurement is taken. However, away from the end points, the fluid distribution is homogeneous when averaged over lengths larger than the percolation correlation length. Then assuming capillary equilibrium, the relative permeability could be defined and measured. In a system where viscous and gravity effects are important, the effective percolation probability will change by ~ 1 over a distance $L_t = 1/C_A$ or $1/B$, respectively. This distance is in the range 10^4 – 10^6 pore lengths or 1–100 m. It is over this scale that we expect the saturation profile to change appreciably. The effective correlation length ξ , which we define as

$$\frac{1}{\xi} = \frac{1}{L} + \frac{1}{\xi_B} + \frac{1}{\xi_V} \quad (6.23)$$

in extension to Eq. (6.11), is much smaller than L_t . Thus if we measure k_r over a length L , where $L_t \gg L \gg \xi$, the saturation is approximately constant and the relative permeability will be close to the steady state or $B=0$ value, except for the shift in end points discussed earlier. Thus, even in displacements dominated macroscopically by viscous forces, the relative permeability concept is still valid, since relative permeability may be measured over a range of lengths where the saturation distribution is homogeneous and the local fluid configuration is determined by capillary equilibrium. However, relative per-

meabilities are used in reservoir simulators and are defined in computational grid blocks often 100 m across, which may be larger than L_t . Over these lengths, gravitational and viscous instabilities may develop, leaving large unswept regions. k_r in these circumstances must be a “renormalized” function, which accounts for both the small-scale physics and the effects of viscous fingering and reservoir heterogeneity over larger distances. This approach has been pursued for miscible flow [83] and recently for immiscible displacement [84].

VII. SECONDARY DRAINAGE AND IMBIBITION

So far we have only discussed primary drainage and imbibition, where the rock originally contains just one fluid. More normally, samples from reservoirs contain both wetting and nonwetting phases, whose distribution represents the terminal point of a primary drainage.

An exhaustive and excellent discussion of secondary displacements, using network modeling to predict the relative permeabilities and capillary pressures, which are then compared with experimental results on representative samples, is given by Jerauld and Salter [13]. In this section we will briefly present some results from the simulation of secondary displacements in a network model.

A. Simulations of secondary displacement

We will simulate the sequence of floods that a sample undergoes during standard laboratory analysis:

(i) *Primary drainage*— nonwetting fluid is injected into a sample containing only wetting fluid, to initialize the core at an initial oil saturation.

(ii) *Secondary imbibition*— wetting fluid is injected into a sample after primary drainage to mimic water flooding in a reservoir.

(iii) *Secondary drainage*— nonwetting fluid is injected after a secondary imbibition to determine the trapping of oil which may encroach from another portion of the reservoir.

We perform simulations of primary displacements as described in Secs. IV and V. The final fluid distributions in each case are stored. Then the injection of a wetting or nonwetting fluid is simulated using the displacement mechanisms described in the previous sections.

As an example, Fig. 27 shows the relative permeability curves for primary drainage with trapping in pores, followed by secondary imbibition by “snap-off” and I_1 and then secondary drainage on a $16 \times 16 \times 16$ network. The displacement mechanisms in drainage and imbibition are very different, which means that the secondary relative permeability curves do not follow the primary curves back to 100% wetting phase. The filling of pores by I_1 resembles a cluster growth mechanism, rather than a percolation model. Thus the relative permeability at a given pore occupancy in imbibition is very different from drainage, which we can model by a percolation process. The feature is called hysteresis and is also seen in the capillary pressure curves, Fig. 28. In strongly wetting systems the hysteresis is influenced by the ratio of pore to

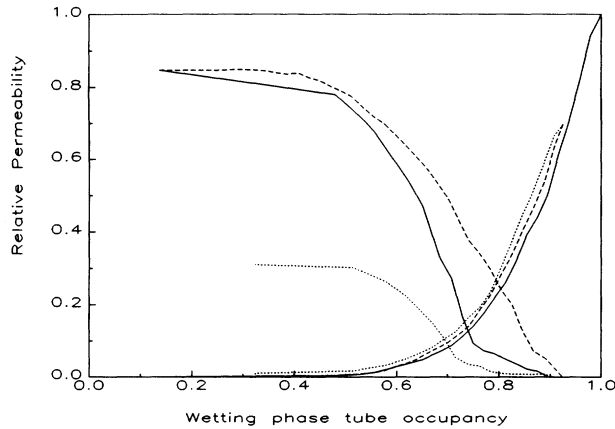


FIG. 27. Relative permeability hysteresis computed on a $16 \times 16 \times 16$ network as a function of tube occupancy. Primary drainage with trapping (solid line) is followed by imbibition by “snap-off” and I_1 (dashes), followed by secondary drainage (dots).

throat size and local pore- and throat-size correlations [13] and has been observed experimentally by many investigators [48,60,85–92].

VIII. CONCLUSIONS

We have reached several conclusions, as follows:

(i) In drainage, film flow or flow along microscale roughness of the wetting phase is essential to allow the nonwetting phase to form well-connected pathways through the system. With no film flow at all, the relative permeability of the invading phase is essentially zero, regardless of saturation. We identify two types of realistic displacement: flow with trapping pores, where the wetting phase cannot drain from large volumes surrounded by nonwetting fluid, and no trapping, where all the wetting phase may escape along microscopic channels and the irreducible saturation is close to zero. We have computed example relative permeabilities in both cases and discussed the circumstances in which each mechanism is likely to be seen.

(ii) We verified the percolation theory results of Wilkinson [33] for a model with the correct pore-scale displacement processes in drainage, and for trapping in drainage and imbibition. The percolation exponents are unaffected by trapping, or the detail of the pore structure.

(iii) We postulated an effective correlation length for

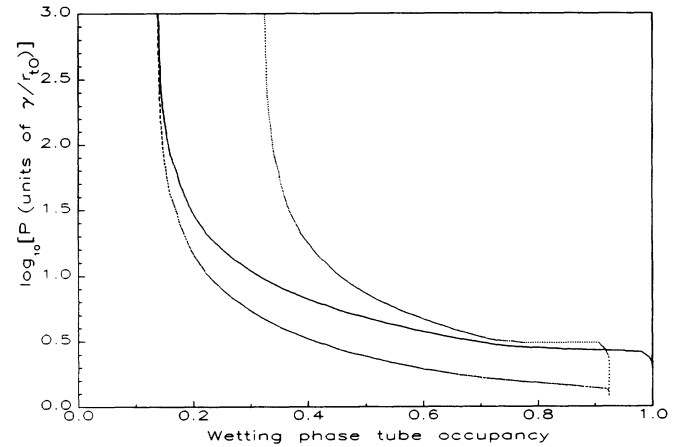


FIG. 28. Capillary pressure hysteresis for the computation described in Fig. 27 as a function of tube occupancy. The wetting phase is assumed to be at zero pressure.

finite-sized systems reduced by gravity and viscous forces, and verified by simulation Wilkinson’s percolation theory predictions for the effect of buoyancy on trapped saturation. For both drainage and imbibition, the change in residual saturation is consistent with finite-size percolation theory.

(iv) The saturation profile changes by ~ 1 over a macroscopic length L_t , which is the scale at which buoyancy and/or viscous forces become larger than the capillary pressure. There is also a smaller correlation length ξ below which the fluid configuration may be percolation-like and above which the saturation distribution is approximately homogeneous, while slowly varying over L_t . We define and measure mesoscopic parameters such as relative permeability and capillary pressure over a scale L . If $L_t \gg L \gg \xi$, then the relative permeability is only perturbed from its value in a steady-state flow at capillary equilibrium and is a well-defined intensive property of the system. This gives the description of multiphase displacements in macroscopic, spatially heterogeneous porous media a firm theoretical basis.

ACKNOWLEDGMENTS

We are grateful for useful help from and discussions with David Wilkinson, John Williams, Peter King, Ken Sorbie, Conor O’Carroll, and Stephen MacDougal.

*Present address: Department of Petroleum Engineering, Stanford University, Stanford, CA 94305-2220.

- [1] I. Fatt, *Trans. AIME* **207**, 144 (1956).
- [2] A. C. Payatakes, *Ann. Rev. Fluid Mech.* **14**, 365 (1982).
- [3] J-D. Chen and J. Koplik, *J. Coll. Int. Sci.* **108**, 304 (1985).
- [4] J-D. Chen and D. Wilkinson, *Phys. Rev. Lett.* **55**, 1892 (1985).
- [5] J. D. Sherwood and J. Nittmann, *J. Phys. (Paris)* **47**, C2-15 (1986).
- [6] P. R. King, *J. Phys. A* **20**, L529 (1987).
- [7] M. J. Blunt and P. R. King, *Phys. Rev. A* **37**, 3935 (1988).
- [8] R. Lenormand and C. Zarcone, *Transport in Porous Media* **4**, 599 (1989).
- [9] C. E. Diaz, I. Chatzis, and F. A. L. Dullien, *Transport in Porous Media* **2**, 215 (1987).
- [10] L. Furuberg, J. Feder, A. Aharony, and T. Jøssang, *Phys. Rev. Lett.* **61**, 2117 (1988).
- [11] P. G. Toldeo, L. E. Scriven, and H. T. Davis, *Society of Petroleum Engineers No. 19618*, in *Proceedings of the 64th Ann. Tech. Conf. of the SPE, San Antonio TX (SPE,*

- Richardson, TX, 1989).
- [12] C. D. Tsakiroglou and A. C. Payatakes, *J. Colloid Int. Sci.* **137**, 135 (1990).
- [13] G. R. Jerauld and S. J. Salter, *Transp. Porous Media* **5**, 103 (1990).
- [14] J. Koplik and T. J. Lasseter, *Chem. Eng. Commun.* **26**, 285 (1984).
- [15] J. Koplik and T. J. Lasseter, *Soc. Pet. Eng. J. Feb.*, 89 (1985).
- [16] R. Lenormand, E. Touboul, and C. Zarcone, *J. Fluid Mech.* **189**, 165 (1988).
- [17] R. Lenormand, *Proc. R. Soc. London, Ser. A* **423**, 159 (1989).
- [18] R. Lenormand, *Physica* **140A**, 114 (1986).
- [19] M. J. Blunt and P. R. King, *Phys. Rev. A* **42**, 4780 (1990).
- [20] M. J. Blunt and P. R. King, *Transport in Porous Media* **6**, 407 (1991).
- [21] M. Cielpak and M. O. Robbins, *Phys. Rev. Lett.* **60**, 2042 (1988).
- [22] R. Lenormand and C. Zarcone, Society of Petroleum Engineers No. 13264, in Proceedings of the 59th Ann. Tech. Conf. of the SPE, Houston, TX (SPE, Richardson, TX, 1984).
- [23] R. Lenormand and C. Zarcone, *Phys. Rev. Lett.* **54**, 2226 (1985).
- [24] J. P. Stokes, D. A. Weitz, J. P. Gollub, A. Dougherty, M. O. Robbins, P. M. Chaikin, and H. M. Lindsay, *Phys. Rev. Lett.* **57**, 1718 (1986).
- [25] K. J. Måløy, J. Feder and T. Jøssang, *Phys. Rev. Lett.* **55**, 2688 (1985).
- [26] M. M. Dias and A. C. Payatakes, *J. Fluid Mech.* **164**, 337 (1986).
- [27] A. A. Heiba, M. Sahimi, L. E. Scriven, and H. J. Davis, Society of Petroleum Engineers No. 11015, in Proceedings of the 57th Ann. Tech. Conf. of the SPE of AIME, New Orleans, LA (SPE, Richardson, TX, 1982).
- [28] R. Chandler, J. Koplik, K. Lerman, and J. F. Willemsen, *J. Fluid Mech.* **119**, 249 (1982).
- [29] D. Wilkinson and J. F. Willemsen, *J. Phys. A* **16**, 3365 (1983).
- [30] B. Nickel and D. Wilkinson, *Phys. Rev. Lett.* **51**, 71 (1983).
- [31] M. M. Dias and D. Wilkinson, *J. Phys. A* **19**, 3131 (1986).
- [32] J. F. Willemsen, *Phys. Rev. Lett.* **52**, 2197 (1984).
- [33] D. Wilkinson, *Phys. Rev. A* **34**, 1380 (1986).
- [34] D. Wilkinson, *Phys. Rev. A* **30**, 520 (1984).
- [35] R. Lenormand, *C. R. Acad. Sci. Ser. B* **297**, 437 (1983).
- [36] R. Lenormand (unpublished).
- [37] D. Y. C. Chan and B. D. Hughes, *Phys. Rev. A* **38**, 4106 (1988).
- [38] M. Muskat and M. W. Meres, *Phys.* **7**, 346 (1936).
- [39] R. D. Wyckoff and H. G. Botset, *Phys.* **7**, 325 (1936).
- [40] H. Darcy, *Les Fontaines Publiques de la Ville de Dijon* (Dalmont, Paris, 1856).
- [41] M. C. Leverett, *Trans. AIME* **142**, 152 (1941).
- [42] M. Danis and C. Jacquin, *Revue de l'Institut Français du Pétrole* **38**, 723 (1984).
- [43] M. Danis and M. Quintard, *Revue de l'Institut Français du Pétrole* **39**, 37 (1984).
- [44] B. J. Bourblaux and F. Kalaydjian, *Soc. Pet. Eng. Reservoir Eng.* **4**, 361 (1990).
- [45] C. Bardon and D. Longeron, *Soc. Pet. Eng. J.* **20**, 391 (1980).
- [46] F. A. L. Dullien, *Porous Media: Fluid Transport and Pore Structure* (Academic, New York, 1979).
- [47] J. O. Amefule and Handy L. L., *Soc. Pet. Eng. J.* **22**, 371 (1982).
- [48] J. S. Osaba, J. G. Richardson, J. K. Kerver, J. K. Hafford, and P. M. Blair, *Pet. Trans. AIME* **191**, 47 (1951).
- [49] J. G. Richardson, J. M. Kerver, J. K. Hafford, and J. S. Osaba, *Pet. Trans. AIME* **195**, 187 (1952).
- [50] C. R. Sandberg, L. S. Gournay, and R. F. Sipple, *Trans. AIME* **213**, 361 (1958).
- [51] A. Labastie, M. Guy, J. P. Declaud, and R. Iffy, Society of Petroleum Engineers No. 9226, in Proceedings of the 56th Ann. Tech. Conf. of the SPE, Dallas, TX (SPE, Richardson, TX, 1980).
- [52] I. Chatzis and F. A. L. Dullien, *Int. Chem. Eng.* **25**, 47 (1985).
- [53] I. Chatzis and F. A. L. Dullien, *Powder Technol.* **29**, 117 (1981).
- [54] D. Stauffer, *Introduction to Percolation Theory* (Taylor and Francis, London, 1985).
- [55] J. W. Essam, *Rep. Prog. Phys.* **43**, 833 (1980).
- [56] Z. Dagan, S. Weinbaum, and P. Pfeffer, *J. Fluid Mech.* **115**, 505 (1982).
- [57] C.-E. Froberg, *Introduction to Numerical Analysis* (Addison-Wesley, Reading, MA, 1981).
- [58] S. L. Bryant and M. J. Blunt, *Phys. Rev. A* **46**, 2004 (1992).
- [59] M. C. Leverett, *Trans. AIME* **132**, 149 (1938).
- [60] P. Ramondi and M. A. Torasco, *Soc. Pet. Eng. J.* **4**, 49 (1964).
- [61] J. T. Morgan and D. T. Gordon, *J. Petrol. Tech.* **22**, 1199 (1970).
- [62] M. Muskat, R. D. Wyckoff, H. G. Botset, and M. W. Meres, *Trans. AIME* **123**, 69 (1937).
- [63] S. J. Salter and K. K. Mohanty, Society of Petroleum Engineers No. 11017, in Proceedings of the Fourth Symposium on Enhanced Oil Recovery, Tulsa, OK (SPE, Richardson, TX, 1984).
- [64] F. A. L. Dullien, G. K. Lai, and I. F. MacDonald, *J. Colloid Interface Sci.* **109**, 201 (1986).
- [65] J. C. Melrose (unpublished).
- [66] C. C. Mattax and J. R. Kyte, *Oil Gas J.* **59**, 115 (1961).
- [67] J. J. Pickell, B. F. Swanson, and W. B. Hickman, *Soc. Pet. Eng. J.* **6**, 55 (1966).
- [68] J. G. Roof, *Soc. Pet. Eng. J.* **10**, 85 (1970).
- [69] I. Chatzis, N. R. Morrow, and H. T. Lim, *Soc. Pet. Eng. J.* **23**, 311 (1983).
- [70] Y. Li and N. C. Wardlaw, *J. Colloid Interface Sci.* **109**, 461 (1985).
- [71] Y. Li and N. C. Wardlaw, *J. Colloid Interface Sci.* **109**, 473 (1985).
- [72] K. K. Mohanty, T. Davis, and L. E. Scriven, *Soc. Pet. Eng. Reservoir Eng.* **1**, 113 (1987).
- [73] I. Chatzis and F. A. L. Dullien, *J. Colloid Interface Sci.* **91**, 199 (1982).
- [74] Y. Li, W. G. Laidlaw, and N. C. Wardlaw, *Adv. Colloid Interface Sci.* **26**, 1 (1986).
- [75] K. K. Mohanty, T. Davis, and L. E. Scriven, Society of Petroleum Engineers No. 9406, in Proceedings of the 55th Ann. Tech. Conf. of the SPE, Dallas, TX (SPE, Richardson, TX, 1980).
- [76] K. O. Meyers and S. J. Salter, No. 12696, in Proceedings of the Fourth Symposium on Enhanced Oil Recovery, Tulsa, OK (SPE, Richardson, TX, 1984).
- [77] E. G. Mathers and R. A. Dawe (unpublished).

- [78] D. Wilkinson and M. Barsony, *J. Phys. A* **17**, L129 (1984).
- [79] T. Jøssang, in *Proceedings of the European Conference of the Mathematics of Oil Production, Cambridge, July 1989*, edited by P. R. King (Clarendon, Oxford, 1992).
- [80] A. Birovljev, L. Furuberg, J. Feder, T. Jøssang, K. J. Måløy, and A. Aharony, *Phys. Rev. Lett.* **67**, 584 (1991).
- [81] W. H. J. Childs, *Physical Constants* (Methuen, London, 1949).
- [82] D. Wilkinson, private communication.
- [83] M. I. Morris and R. C. Ball, *J. Phys. A* **23**, 4199 (1990).
- [84] P. R. King, *Transp. Porous Media* (to be published).
- [85] T. M. Geffen, W. W. Owens, D. R. Parrish, and I. Morse, *Pet. Trans. AIME* **192**, 99 (1951).
- [86] J. Naar, R. J. Wygal, and J. H. Henderson, *Soc. Pet. Eng. J.* **2**, 13 (1962).
- [87] A. W. Talash, Society of Petroleum Engineers No. 5810, in *Proceedings of the Symposium on Improved Oil Recovery*, Tulsa, OK (SPE, Richardson, TX, 1976).
- [88] R. A. Fulcher, T. Ertekin, and C. D. Stahl, *Soc. Pet. Eng. J.* **25**, 249 (1985).
- [89] M. R. Hopkins and K. M. Ng, *Chem. Eng. Commun.* **46**, 253 (1986).
- [90] A. Poulavassilis, *Soil Sci.* **109**, 5 (1970).
- [91] G. C. Topp and E. E. Miller, *Soil. Sci. Soc. Am. Proc.* **30**, 156 (1966).
- [92] T. Talsma, *Water Resour. Res.* **6**, 964 (1970).

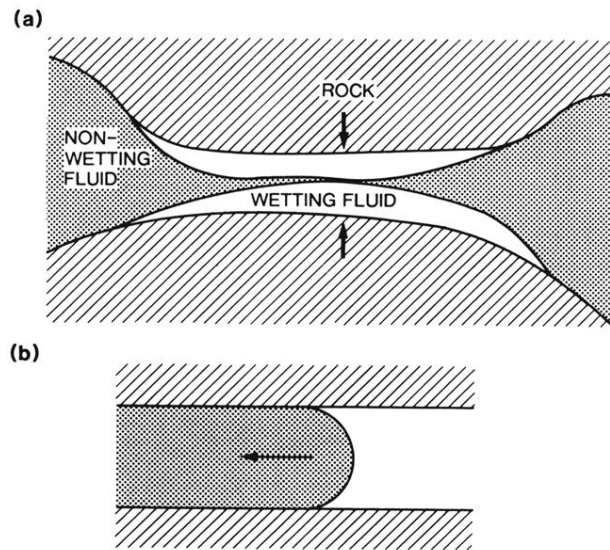


FIG. 12. Displacement processes in imbibition. (a) "Snap-off." (b) Pistonlike displacement.

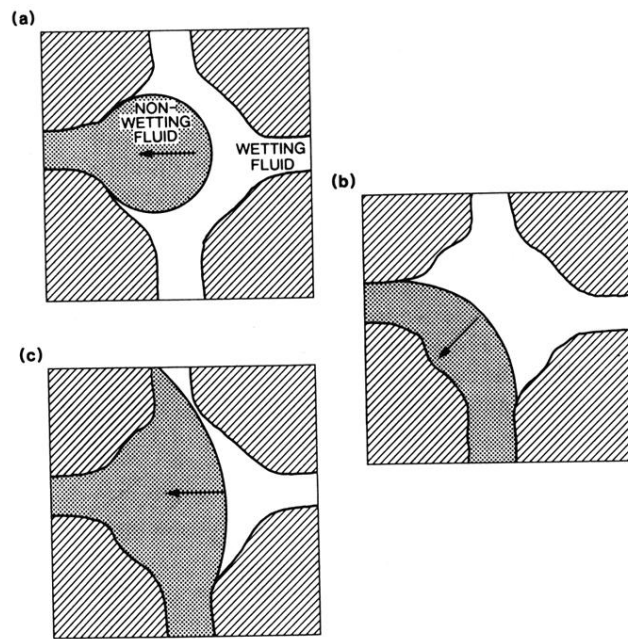


FIG. 14. Mechanisms of pore filling in imbibition in a four-fold-coordinated lattice. (a) I_1 . (b) I_2 . (c) I_3 . I_4 is not possible if the pores are larger than the throats.

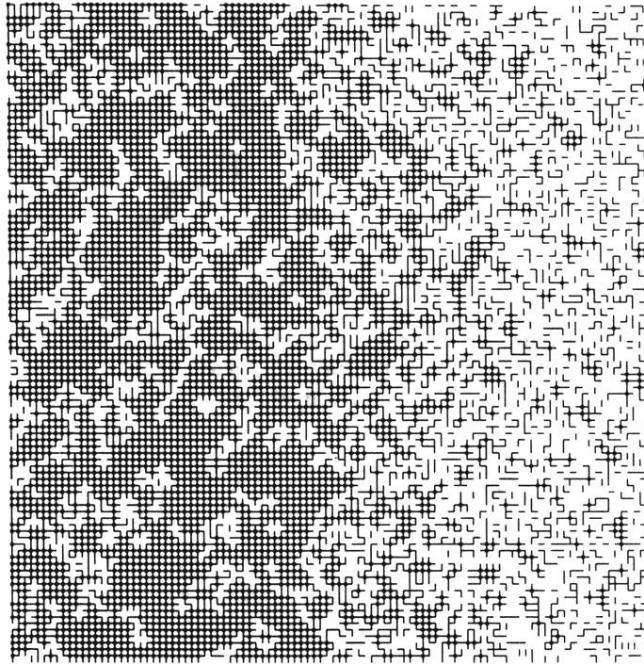


FIG. 18. Imbibition at intermediate capillary number on a 100×100 square network. Pores and tubes completely filled by injected fluid are shown. The width of the advancing wetting film (which is not shown) is approximately 100 tube lengths. We see a ragged frontal advance near the inlet, preceded by some pore and tube filling, where the fluid is supplied by film flow.